

https://dspace.org/

Fracture of plain concrete: a comparative study of notched beams of varying depth

Alexander, Mark Gavin

2014-09-12
http://hdl.handle.net/10539/15527

Downloaded from a DSpace repository. https://dspace.org/

3.3.1 CRITICAL STRESS-INTENSITY FACTOR

The stress-intensity factor K describes the elastic stress field in the vicinity of a crack tip. It is a single parameter measure of the mechanical properties of a material in the presence of a crack (in much the same way that stress characterises the mechanical properties of a material without a crack). The distribution of stresses in the vicinity of a crack are governed predominantly by the geometry of the crack itself, since the surfaces of the crack are stress-free boundaries of the body near the crack tip. Remote boundaries and loading forces affect only the intensity of the crack tip stress field (i.e. the value of K) and not its form. The higher the value of K the more severe the crack, and when a critical value K_c is reached, the crack will extend. K_c may therefore be regarded as a measure of a material's fracture toughness or resistance to brittle fracture.

In general terms, K can be written as:-

$$K = \alpha\sigma\sqrt{(\pi c)} \qquad (3.1)$$

where α is a geometric correction factor, σ is the applied global stress, and c is the flaw or crack size. K thus has units of stress x length$^{\frac{1}{2}}$ (eg. MPa$\sqrt{m}$).

In appropriate circumstances, K_c could be used to calculate the load that a structural member containing a flaw of known size could sustain without fracture. An important property of K is that the total K value due to superimposed stress fields is a linear addition of the K values of the individual stress fields. It thus has application to problems involving a combination of loadings.

Investigators in the metallic field have recognised that the experimental evaluation of K_c assumes a high degree of elastic constraint to plastic flow of the material at the crack tip. This implies that provided yielding and other non-linear effects such as microstructural irregularities are confined to a small region

at the crack tip, the elastic stresses outside this region are only slightly affected, and the stress-intensity factor still provides a reasonable description of the crack tip stress field. A plastic zone size factor is used as a criterion for this condition. Where lower constraint occurs such as in a thin plate, the effective toughness of the material can be substantially greater than K_c. This is basically a plane stress/plane strain problem, and the fracture toughness for metallic materials can alter enormously according as the elastic-plastic stress field ahead of the crack approximates to plane stress or plane strain conditions. K_c implies plane strain conditions, i.e. a heavy section with adequate dimensions, and gives a lower limit to the fracture toughness. Most investigators in the non-metallic field have assumed plane strain conditions exist during tests on notched specimens. It appears that this problem has not received much attention, but Hillerborg[45] states that plane strain is the prevailing condition in normal tests on cemented materials.

FORMULA FOR K_c

The methods of obtaining an expression for K (i.e. a K calibration) are based either on experiment, in which measurements are made of compliance (reciprocal of stiffness) of a specimen with a crack incrementally extended between successive measurements, or on mathematical stress analysis in which a mathematical model is constructed to suit the specimen design. The mathematical technique involves a boundary value collocation procedure in which a suitable stress function χ is formed which satisfies the biharmonic equation $\nabla^4\chi=0$ and the boundary conditions at a finite number of points along the boundaries of the specimen. The results may be expressed in polynomial form that permits calculation of the stress-intensity factor in terms of applied load and specimen dimensions. Alternatively, finite element techniques may be employed to derive a K expression.

Brown and Srawley[44] have reported a relationship between K and the specimen dimensions and loading for a centre-notched beam in pure

bending (four-point bending) and in three-point bending, as follows:-

$$K = Y \frac{6M\sqrt{c}}{bd^2} \qquad (3.2)$$

where $Y = A_0+A_1(c/d)+A_2(c/d)^2+A_3(c/d)^3+A_4(c/d)^4$ (3.3)

M is the bending moment in three-point or four-point bending, and b,d are specimen breadth and depth respectively.

K is a function of a fourth-degree polynomial in the notch depth ratio c/d. K is accurate to within 0,2 per cent for all values of c/d up to 0,6. The coefficients A are given in table 3.1, the values being dependent on the type of bending in the specimen.

Table 3.1 Values of the coefficients A for calculating Y

		A_0	A_1	A_2	A_3	A_4
Pure bending		+ 1,99	- 2,47	+ 12,97	- 23,17	+ 24,80
Three-point:	S/d=8	+ 1,96	- 2,75	+ 13,66	- 23,98	+ 25,22
	S/d=4	+ 1,93	- 3,07	+ 14,53	- 25,11	+ 25,80

(S = major support span)

Strictly, the expression for K in (3.2) above refers to beams which are rectangular in elevation and of constant section. In the present tests, beams which had constant and variable sections were used, and details are given in chapter 4. A constant ratio of span/depth (at mid-span) of four was used throughout. Figure 3.2 shows a constant section beam of the type used in the tests, together with the expression for K.

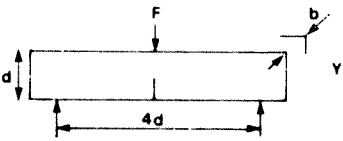

$$Y = \frac{Kbd}{6Fc^{1/2}} = 1.93 - 3.07\left(\frac{c}{d}\right) + 14.53\left(\frac{c}{d}\right)^2 - 25.11\left(\frac{c}{d}\right)^3 + 25.80\left(\frac{c}{d}\right)^4$$

$$\left(\frac{c}{d} \leq 0.6\right)$$

Figure 3.2 Edge-notched constant section beam loaded in three-point bending

The depth of the variable section beams used in the tests varied along the beam length, and it was therefore necessary to consider whether a modification of the K expression for a suitable effective span/depth ratio for these beams was required. Reference to table 3.1 will show that the difference between the values of Y for the different conditions of bending are small amounting to about 3 per cent between S/d = 8 and S/d = 4. This is consistent with an earlier remark that K will be very little affected by specimen geometry and loading but critically affected by the geometry of the crack itself. It was therefore considered unnecessary to perform an entire stress analysis for the variable section beams which had a variable span/depth ratio. Since the stress analysis procedure for obtaining K is based on determining the deformations of the specimen in the presence of a crack and under given loading, it was considered that the best estimate for an effective span/depth ratio of the variable section beams could be obtained by calculating the depth of a constant section beam which would exhibit the identical deformation (i.e. deflection behaviour as that of a variable section beam. This depth could then be considered as the effective depth of the variable section beam, from which an effective span/depth ratio could be obtained. This procedure was carried out and the effective span/depth ratio for the variable section beams was found to be 5,45 (see appendix E). Using this value together with a linear interpolation between A values for S/d = 4 and 8, it was found that the difference between Y values for S/d = 4 and 5,45 was only 1,3 per cent (for c/d = 0,4). In view of this very small

difference, it was decided to use the K expression for S/d = 4 for the constant and variable section beams used in the tests. It might be noted that use of span/depth ratios equal to or greater than four avoids a deep beam condition. (Details of the dimensions used for the test beams can be found in chapter 4 (figure 4.1)).

Note that equation (3.2) is no longer valid for c/d > 0,6. A useful solution for this condition has been proposed by Mai et al[43], based on work by Winne and Wundt[61]. According to later equations (3.19) and (3.20), K can be expressed as:-

$$\frac{K}{\sigma_n h^{\frac{1}{2}}} = \left[(1-\nu^2)\ f\left(\frac{c}{d}\right)\right]^{\frac{1}{2}} \qquad (3.4)$$

where σ_n is the net stress at the root of a notch or crack,

and h = d-c, termed the residual ligament depth.

Values for f(c/d) are given in later figure 3.5 (from Winne and Wundt[61]), from which it can be seen that for deep notching (i.e. c/d > 0,5), f(c/d) tends asymptotically to a value of 0,521. Equation (3.4) then reduces to:-

$$\frac{K}{\sigma_n h^{\frac{1}{2}}} = \left[(1-\nu^2)\ 0{,}521\right]^{\frac{1}{2}} \qquad (3.5)$$

Since ν (Poisson's ratio) for concrete is typically about 0,15, the $(1-\nu^2)^{\frac{1}{2}}$ term above equals unity for practical purposes, and equation (3.5) reduces to:-

$$\frac{K}{\sigma_n h^{\frac{1}{2}}} = 0{,}72 \qquad (3.6)$$

In order to compare equation (3.6) with the Brown and Srawley equation (3.2), the latter equation can be expressed in the following form:-

$$K = Y \frac{6M}{bd^2} c^{\frac{1}{2}}$$
$$= Y \sigma c^{\frac{1}{2}}$$

where $\sigma = \frac{6M}{bd^2}$ is the nominal stress based on gross section area.

The relationship between σ and σ_n is:-

$$\sigma = \sigma_n \left(\frac{h}{d}\right)^2$$

Therefore, we can express equation (3.2) as

$$K = Y c^{\frac{1}{2}} \sigma_n \left(\frac{d-c}{d}\right)^2$$

or

$$\frac{K}{\sigma_n (d-c)^{\frac{1}{2}}} = Y c^{\frac{1}{2}} \frac{(d-c)^{\frac{1}{2}}}{d^2}$$

$$= Y \frac{c}{d}^{\frac{1}{2}} \left(\frac{d-c}{d}\right)^{\frac{1}{2}}$$

Finally

$$\frac{K}{\sigma_n h^{\frac{1}{2}}} = Y \frac{c}{d}^{\frac{1}{2}} \left(\frac{1-c}{d}\right)^{\frac{1}{2}} \qquad (3.7)$$

Equations (3.7) and (3.6) are plotted as functions of (c/d) in figure 3.3. The Brown and Srawley solution begins to reduce rapidly at c/d > 0,6, while the Winne and Wundt solution is still well above the more accurate Brown and Srawley solution at c/d = 0,5. Therefore, a modified solution as shown in figure (3.3) is proposed, such that for c/d values greater than 0,5, the stress intensity expression becomes:-

$$\frac{K}{\sigma_n h^{\frac{1}{2}}} = 0,194 \frac{c}{d} + 0,528 \qquad (3.8)$$

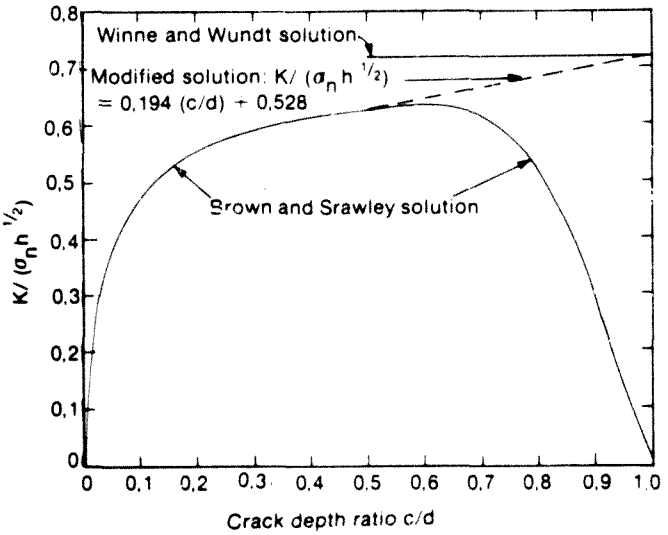

Figure 3.3 Solutions for stress-intensity factor in notched beams

Equation (3.8) can be used to infer effective Y values for direct use in equation (3.2). From equation (3.7):-

$$Y = \frac{K}{\sigma_n h^{\frac{1}{2}}} \left[\left(\frac{c}{d}\right)^{\frac{1}{2}} \left(1-\frac{c}{d}\right)^{\frac{3}{2}} \right]^{-1} \qquad (3.9)$$

and substituting from equation 3.8:-

$$Y_{eff} = \frac{0,194(c/d) + 0,528}{\left(\frac{c}{d}\right)^{\frac{1}{2}} \left(1-\frac{c}{d}\right)^{\frac{3}{2}}} \qquad (3.10)$$

Hence, Y values can be found from equation (3.3) for $c/d \leq 0,5$ using coefficients for three-point bending from table 3.1, and from equation (3.10) for $c/d > 0,5$. For $c/d > 0,8$, Mai et al[43] point out that end effects will adversely influence results, and therefore equations (3.8) and (3.10) should be regarded as valid for $0,5 < c/d < 0,8$. The two equations for Y are shown plotted in figure 3.4, for the particular test geometry that was used.

3.3.2 CRITICAL STRAIN ENERGY RELEASE RATE

The use of this fracture parameter G_c is based on evaluating the rate of strain energy release at the point of fracture. Irwin[62] originally argued that if the fracture process was essentially similar for different loadings and geometries, the fracture event would occur when the strain energy release rate reached a critical value, that value when energy release more than compensated for energy demand from fracture surfaces. This critical value could be regarded as a material property to be determined by a fracture test. Irwin also suggested that the critical strain energy release rate could be interpreted as a force, defined as the irreversible energy loss per unit area of newly created surface. The critical value of this force G is denoted G_c, and applies when the crack starts to propagate. Referring to figure 2.2, the strain energy released by the crack in advancing to a length of c is:-

$$U = \frac{\pi\sigma^2 c^2}{E} \qquad (3.11)$$

The rate of release of strain energy with crack advance is

$\frac{\partial U}{\partial c}$, denoted G, i.e.

$$G = \frac{2\pi\sigma^2 c}{E} \qquad \text{(plane stress)} \qquad (3.12)$$

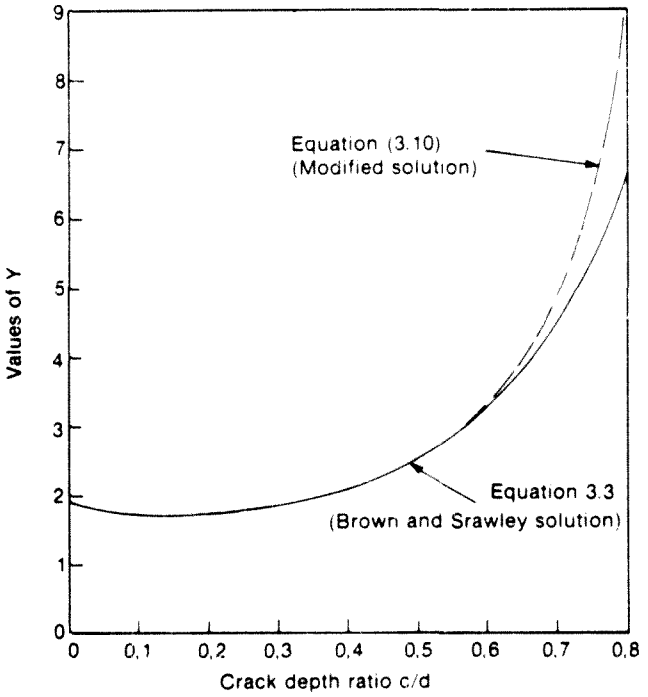

Figure 3.4 Values of Y for calculating stress-intensity factor, three-point bend specimens

Note that the units of G are either Force per unit length, or Work per unit area.

At the critical point of unstable crack propagation, G becomes G_c, the *critical strain energy release rate*, or the critical crack-extension force. G is thus regarded as the driving force behind crack extension. The relationship between G and G_c is the same as that between K and K_c : G is primarily a function of loading and geometry, while G_c is a material property.

FORMULA FOR G_c

A relationship for G_c in a notched beam can be produced by stress analysis, resulting in a mathematical relationship in terms of the specimen dimensions, depth of crack, applied load and modulus of elasticity. G_c is then the value of G in the test at that stress level which causes rapid crack propagation.

The strain energy release rate for plane strain conditions due to a surface crack propagating from a free surface is:-

$$G = \frac{\pi(1-\nu^2)\sigma^2 c}{E} \qquad (3.13)$$

For shallow notches ($c << d$), σ may be regarded as the maximum tensile bending stress at the extreme fibre of the beam.
Thus, for a rectangular beam of width b:-

$$\sigma = \frac{6M}{bd^2} \qquad (M = \text{applied moment}) \qquad (3.14)$$

The net stress at the root of the notch is:-

$$\sigma_n = \frac{6M}{bh^2} \qquad (3.15)$$

where $h = d-c$. Therefore:

$$\sigma^2 = \sigma_n^2 \frac{h^4}{d^4} \tag{3.16}$$

Substituting in (3.13) gives:-

$$G = \frac{\pi(1-\nu^2)}{E} \sigma_n^2 c \frac{h^4}{d^4} \tag{3.17}$$

Now, $h = d-c$, and so we can express this as follows:-

$$\begin{aligned} c\frac{h^4}{d^4} &= c \frac{(d-c)^4}{d^4} = c \left(\frac{d-c}{d}\right)^4 \\ &= c \left(\frac{d-c}{d}\right)\left(\frac{1-c}{d}\right)^3 \\ &= h \frac{c}{d}\left(\frac{1-c}{d}\right)^3 \end{aligned} \tag{3.18}$$

Therefore, G may be written as:-

$$G = \frac{(1-\nu^2)}{E} \sigma_n^2 h \left[\pi \frac{c}{d}\left(\frac{1-c}{d}\right)^3\right]$$

or $$G = \frac{(1-\nu^2)}{E} \sigma_n^2 h f\left(\frac{c}{d}\right) \tag{3.19}$$

where $f\left(\frac{c}{d}\right) = \pi \frac{c}{d}\left(\frac{1-c}{d}\right)^3$

This formula only applies to shallow notches of $c/d < 0,15$.
For deeply notched beams, the effects of the reduced cross-section and the non-uniformity of stresses must be taken into account. The most useful solution for this is the f(c/d) curve proposed by Winne and Wundt[61]. This curve is shown in figure 3.5. It is seen that for deep notching, i.e. $c/d > 0,5$, f(c/d) tends to a value of 0,521.

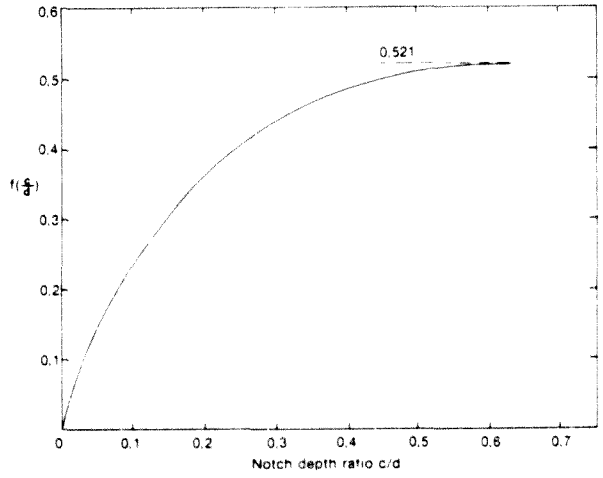

Figure 3.5 Curve for calculating G for notched beams (from ref. 61)

RELATION BETWEEN K AND G

Irwin originally showed that crack growth occurring at a critical value of K was equivalent to satisfying the two necessary conditions for fracture discussed in section 2.2, viz. energetic desirability for crack propagation, and molecular mechanism of crack growth. Hence, it can be shown for LEFM that there is a simple relationship between K and G:-

$$K^2 = EG \quad \text{(plane stress)} \tag{3.20}$$

$$K^2 = \frac{EG}{(1-\nu^2)} \quad \text{(plane strain)}$$

where E is Young's Modulus and ν is Poisson's Ratio.

Examination of the Griffith equation (equation (2.2)) and equation (3.13) reveals that for LEFM, a relationship also exists between the surface energy γ and G, viz.

$$G = 2\gamma \tag{3.21}$$

This relation strictly holds only for brittle elastic materials which fracture catastrophically at first crack propagation[63].

Both K_c and G_c were evaluated in the present tests.

3.4 SLOW CRACK GROWTH AND BEAM COMPLIANCE

One of the prima ~ differences between fracture testing of metals and cemented materials is the degree of slow stable crack growth from a notch prior to rapid crack propagation. The greater the degree of slow crack growth the more removed does the test become from the assumption of LEFM and the Griffith approach. To counter this, the standard plane strain fracture toughness test for metals of the American Society for Testing and Materials (ASTM E-399)[68] specifies that the difference between the maximum load in a fracture test and a load obtained by the intersection of the test record (usually a load vs. crack mouth displacement record) and a line with an offset slope of 5 per cent from the initial linear portion of the record should not exceed 10 per cent. For cemented materials this requirement is usually not met, except possibly in the case of hardened cement paste. For mortar and concrete, the difference between the two loads mentioned above may be of the order of 30 to 40 per cent. This is due primarily to slow crack growth which is extensive in these types of material . In addition, it is possible by deep notching to create an entirely stable fracture in which no true spontaneous or rapid crack propagation occurs. Hence the problem of slow crack growth is inherent in cemented materials, and cannot be ignore In fact, Cook and Crookham[44] boldly state that the majority of the reported fracture work on concrete suffers from

the shortcoming of not allowing for slow crack growth from the tip of the notch before maximum load is reached. Failure to account for this will cause the calculated fracture parameters to be underestimated.

Having established the importance of accounting for slow crack growth, the question is how is this done? While the question is simple enough, the answer is very much more difficult, due to the complex and tortuous nature of cracking in cemented materials. It is possible to use a microscopic technique[38] to follow the progress of cracking, but crack branching and tortuosity as well as material opacity will affect the result, and microcracking ahead of the visible crack tip cannot readily be observed. An alternative technique is the compliance method, which will be discussed in more detail here. However, it is true to say that to date no really satisfactory method of assessing slow crack growth easily, quickly, and accurately has been devised, and there is even the question of whether this will ever be possible in view of the heterogeneous nature of the materials involved.

The compliance technique for monitoring slow crack growth has its origin in an experimental method derived by Irwin and Kies[44] to determine K or G. The relevant equation is:-

$$G = \frac{1}{2} F^2 \frac{d\lambda}{dc} \qquad (3.22)$$

where λ is defined as the compliance of the specimen
in the presence of a notch,
$F = \frac{1}{\lambda} \delta$ (i.e. the reciprocal of stiffness)
and F, δ are specimen load and deflection respectively

The method of finding G in this case involves measuring specimen compliance with notches of varying depths, expressing the compliance as a function of crack depth and then obtaining the derivative of this function with respect to crack depth. The finite width notch is used to simulate a crack during the initial linear elastic

behaviour under load. Welch and Haisman[21] reported that for mortar and concrete beams there was no significant difference between the compliance of beams with wide sawn notches and those with notches cast with rubber formers or special razor blade inserts. They concluded that the initial compliance of the linear elastic portion of a load-deflection curve for cemented materials is independent of notch sharpness, and a general relationship exists between compliance and notch depth, in the absence of slow crack growth.

However, many researchers have pointed out that the compliance of a natural crack of given depth will not be the same as that of a finite width notch of the same depth. This is due to the influence of the microcracked zone ahead of the crack tip and to traction resistance which exerts a closing stress across the crack faces. Researchers seem divided as to the seriousness of the error introduced by assuming that artificial notch compliance equals natural crack compliance. This error will also vary with the type of material, and is likely to be greater in fibre-reinforced and polymer concretes where considerable closing stresses can be exerted on crack faces by fibres and polymer inclusions spanning the crack than in plain concrete where the traction effects may be expected to be smaller. Thus, Velazco et al[38] found that crack lengths observed in fibre reinforced concrete using a microscope-micrometer were considerably larger than those predicted from a theoretical compliance curve based on a model that did not account for traction effects. On the other hand, Brown[24] and Cook and Crookham[44] have maintained, on the basis of experimental work, that a theoretical compliance - notch depth relation appears to be a valid means of determining crack depth up to a notch depth ratio of about 0,35. However, the latter authors appear to be somewhat self-contradictory by stating that a cast notch does not adequately represent a natural crack and therefore fracture toughness measurements will vary with specimen geometry. Another set of workers, Swartz et al[48], endeavoured to determine the suitability of the compliance calibration method to monitor crack growth in plain concrete beams subject to cyclic loading, and concluded that the method was suitable. They based this conclusion on the fact that there was only a small difference (max. 9 per cent) between their

experimental curve and a theoretical curve deduced from finite element analysis. However, their experimental curve was obtained from tests on beams notched with a diamond saw and in which no natural crack growth occurred prior to measuring compliance. Therefore the effect of crack closing stresses was absent in their tests, making this conclusion somewhat questionable. Finally, Hillemeier and Hilsdorf[12] in tests on hardened cement paste, aggregates, and aggregate-paste interfaces used the compliance technique to successfully calculate crack length for various cycles of load. In these tests, the fracture behaviour of the material was far more brittle than is the case in composite cemented materials, implying that crack-closing stress effects were small. The weight of evidence would seem to indicate that the compliance technique is useful and accurate for assessing the critical crack depth at failure in materials that fracture in a brittle fashion, where slow crack growth prior to failure is limited. However, the heterogeneity of multi-phase materials such as mortar and concrete induces considerable crack growth prior to failure, and this cracking is itself complex and heterogeneous. Therefore the compliance resulting from an artificial notch or a natural crack of equal depths in these materials will differ. An attempt has been made in this thesis (chapter 6) to quantify this difference and to examine its significance.

The compliance technique has been well covered by Brown[24], and will be briefly summarised here. The method assumes that the difference between the compliance of the initial linear portion of a load-deflection record and the compliance at, say, maximum load as measured by the inverse of the slope of the straight line joining the origin to the point of maximum load is due to the slow crack growth occurring from the notch prior to maximum load. The method can be extended to measure compliance at any stage during the test and infer crack depth at this stage, and can be coupled to a load-cycling technique in which the crack is slowly advanced through the specimen. Using a compliance-crack depth relationship, changes in compliance can be converted into increments of crack growth. This compliance-crack depth relationship can be obtained theoretically or experimentally. Brown[24] and subsequently Cook and

Crookham[44] obtained experimental relationships, and found that for beam depths of 100mm there was very little scatter of results and that the two relationships were very close to one another. However, once again the effect of crack-closing stresses was absent from these relationships. Brown's method of calculating crack depth was to measure the change in compliance between the first cycle of load with its known notch depth and the subsequent cycle, and then to use the theoretical compliance relationship to obtain the increment of crack growth. Adding this to the initial notch depth gave a value of total crack depth for use in the expression for K. Brown also stated that the non-linearity of the load-displacement plot made the measurement of compliance the least satisfactory part of the analysis. He used a linear approximation to the most nearly straight part of the load-displacement plot for his compliance. In essence, Brown's method has been used for the present tests. However, the conventional compliance as defined and discussed above has been differentiated from a reloading compliance, which is obtained from the slope of the reloading curve at the start of a new cycle of load. Such a compliance accounts for the effect of crack-closing stresses. Experimental conventional and reloading compliance relationships have been derived, and compared with theoretical relationships. (Details of the derivation of the theoretical compliance-crack depth relationships can be found in appendix E).

To conclude this section, it is necessary to account for slow crack growth in fracture beams of cemented materials. The compliance technique offers one possible method of doing this, although the difference in behaviour between artificial notches and natural cracks remains a thorny problem. To quote from Cook and Crookham[44]:- "The dependence of fracture toughness parameters upon crack length and specimen size appears to vary with the test arrangement and the method of analysis applied. The determination of slow crack growth and its necessary incorporation in the analysis should help to clarify this dependence."

3.5 NON-LINEAR FRACTURE MECHANICS (NLFM) PARAMETERS

Since Kaplan[17] first measured fracture parameters of concrete more than twenty years ago, the body of experimental evidence has increased enormously. Many studies have used the LEFM parameters defined above, and have investigated the influence of aggregates, c/w ratio and other mix ratios, air content and pore size, amongst others, on the fracture parameters. As data became available, it became increasingly obvious that the application of LEFM to cemented materials was not without its problems. Great variability in results occurred between different workers, and frequently LEFM relationships appeared invalid. One of the more obvious reasons for this was the fact that the size of the non-linear zone ahead of the main crack was not small in relation to the size of the members being tested, and this alone would render the purely LEFM approach questionable. In addition to the question of member size, other particular problems had to do with the effects of specimen type, and ratio of notch depth to specimen depth. The entire question of the applicability of LEFM to cemented materials has been thoroughly and admirably reviewed by a number of authors, and the papers by Mindess[28], Swamy[54] and Ziegeldorf[59] might be referred to amongst others. The main questions revolve around aspects such as notch-sensitivity and the minimum size of specimen and ratio of flaw size to specimen size that is required before a fracture test can be considered to be valid. The fact that concrete departs markedly from the normal LEFM assumptions of a single crack in a homogeneous isotropic medium further complicates the issue. Mindess has pointed out that certain of the experimental discrepancies can be resolved by accounting for the differences in experimental techniques that were used, eg. the effect of slow crack growth and different machine stiffnesses. However, a full resolution of the difficulties does not appear possible at this point, and therefore increasing attention is being focused on another set of fracture parameters arising from work in the metallic and ceramic fields on materials that manifestly exhibit non-linear fracture behaviour. For present purposes, these parameters are termed non-linear fracture mechanics (NLFM) parameters, and certain encouraging results

have been obtained to date. This is particularly so for fibre-cement and polymer composites, where the application of LEFM is fraught with uncertainty due to excessive non-linear behaviour.

(It might be noted that use of the term "non-linear fracture mechanics" is preferable to the more common term "elasto-plastic fracture mechanics" when cemented materials are being considered, since these materials do not conform to the typical elasto-plastic behaviour of metals. The consequence of this is that approaches developed for metallic materials are not always directly applicable to cemented materials).

Three main fracture parameters are considered in this section:- they are Crack Growth Resistance Curves (R-Curves), the J-integral, and the effective surface energy γ'. R-curves and γ' were evaluated in the present tests. γ' and J-integral are somewhat related, as will be shown in chapter 9. In addition, the question of the size of the non-linear zone ahead of and surrounding the crack in cemented materials was investigated.

3.5.1 CRACK GROWTH RESISTANCE CURVES (R-CURVES)

R-curve analysis was originally developed in the metallic field[66] from fracture mechanics principles to help deal with situations of plane stress where slow stable crack growth is often extensive. Historically, the method dates back to the 1950's and the work of Irwin and Kies and others[3,5,62,66], but its application to cemented materials is relatively new. The method can be used for making instability predictions from determinations of a critical fracture stress as a function of flaw size; it is also used extensively to characterise the resistance to fracture during stable crack growth.

The method involves the continuous measurement of load and slow stable crack growth. The load values are converted to K values (or other suitable values such as G or γ') for the particular loading

and structural configuration. These K values (normally K_I values) can also be thought of as crack growth resistance values, or R values. The resulting plot of K (or R) versus crack growth at the K values is the R-curve.

Returning to the Griffith energy balance equation given in figure 2.2, unstable crack advance occurs when

$$\frac{\partial}{\partial c}(u-s) \geq 0 \qquad (3.23)$$

where u is the energy release and s is the energy requirement for crack advance.
Now $\partial u/\partial c$ can be recognised as G, the strain energy release rate, and $\partial s/\partial c$ can be thought of as the resistance to crack growth, or R. Hence we can re-write equation (3.23) as:

$$G-R \geq 0 \qquad (3.24)$$

which is the criterion for crack advancement. This equation can equally as well be written as $K-R \geq 0$ if R is expressed in terms of stress intensity units. Figure 3.6 shows schematically the variation of K with crack depth under different applied stress levels, σ. Also shown is a typical R-curve for a given initial crack depth c_0. Applying the condition for crack extension ($K-R \geq 0$) to the condition in figure 3.6, crack extension will occur with increasing stress level, but will be arrested when K = R, i.e. when the K and R curves intersect. However, for the K (σ_{max}) curve a point of tangency is reached between the K and R curves, represented by a critical crack extension Δc_c. Any extension of the crack beyond this point will result in unstable crack propagation as K > R from this point onwards.

R-curve analysis is based on the postulate that for a given material and thickness there is a unique relationship between crack growth and the applied stress-intensity factor, this relationship being characterised by the R-curve. The point is made by Heyer[67] that it is a useful test method applicable to the more ductile materials.

R-curve is a function of crack growth, Δc, rather than the absolute crack depth, and can extend well above the plane strain K_c value[55]. The K values calculated from the test represent the driving force required to produce stable crack growth prior to instability, which occurs when the K and R curves reach a point of tangency.

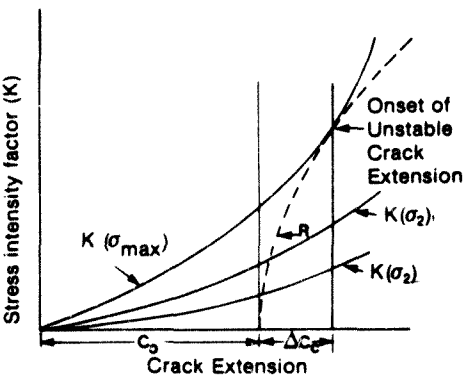

Figure 3.6 Principle of R-curve showing eventual imbalance of stress-intensity factor over resistance to crack extension with increasing stress (σ)

On the assumption that the R-curve is a function of crack growth Δc rather than absolute crack depth, it is possible to show schematically the influence of initial notch depth on K_c. Figure 3.7, taken from ref. 42, indicates that K_c will tend to increase with increasing initial notch depth for materials experiencing slow crack growth prior to ultimate instability. It is interesting to note that Brown[24] found that K_c increased with increasing crack growth for mortar beams, while for paste beams there was essentially no variation of K_c with crack growth. This is consistent with the expectation that slow crack growth would be more extensive in more "ductile" non-linear mortar beams than in brittle paste beams. Unfortunately, Brown does not quote what his initial notch depths were, and therefore a direct interpretation of his results in the light of figure 3.7 is not possible. Figure 3.7 also shows that

there should be a greater amount of slow crack growth in more deeply notched beams than in shallow notched beams.

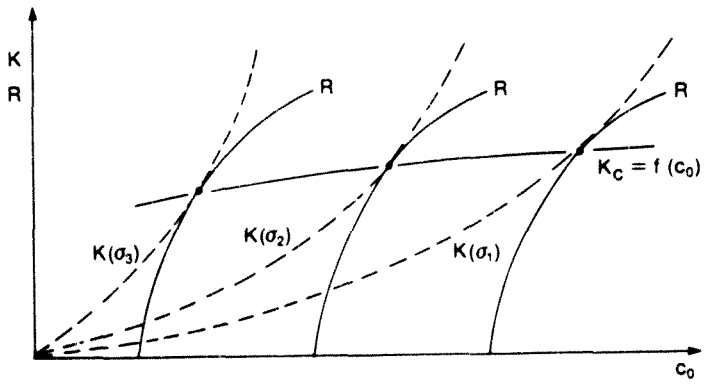

Figure 3.7 Effect of initial notch depth on value of K_C (from ref. 42)

It is interesting to note the differences in interpretation of an R-curve for the metallic and non-metallic cases. In metallic materials, increasing K is necessary to cause the crack to grow under plane stress conditions, and hence the plate thickness will also affect K. In cemented materials (non-metallic), increasing toughness occurs with crack growth primarily due to increase in the zone of microcracking ahead of the crack tip, and to crack-stopping mechanisms. In addition, it is unlikely that a plane stress condition is occurring in the relatively thick specimens used for cemented materials[46]. Hence, the micro-mechanisms represented by R-curves for metals and cemented materials are very different.

It is also interesting to note that the concept of an R-curve as shown in figure 3.6 is very similar to the Glucklich model presented in figure 2.5. Glucklich arrived at his model by considering the increasing resistance to crack growth occurring in a heterogeneous multi-phase material. Hence the concept of an R-curve as representing increasing resistance to crack growth fits in well with our

understanding of the fracture process in heterogeneous cemented materials.

Velazco et al[68] state that R-curve analysis assumes a relationship independent of specimen dimensions and initial crack depth, but certainly for metals the thickness of the specimen will affect the calculated K values. There is still some controversy as to whether R-curves are sensitive to specimen geometry. The method appears to characterise the behaviour of plain and fibre-reinforced concrete very well, as shown by Shah, and co-workers[38,40,41,68,69]. Referring specifically to fracture of plain concrete, Shah and co-workers have shown that it is important to account for the size of the non-linear zone ahead of the main crack in the production of R-curves. This is because the size of this zone can be of similar magnitude to the depth of the visible crack. From results of tests on double torsion and double cantilever specimens, they showed that failure to account for the non-linear zone caused R-curves to be specimen-type dependent whereas R-curves became characteristic of the material itself when this zone size was included in the slow crack growth term. This is shown in figure (3.8), taken from ref. 69.

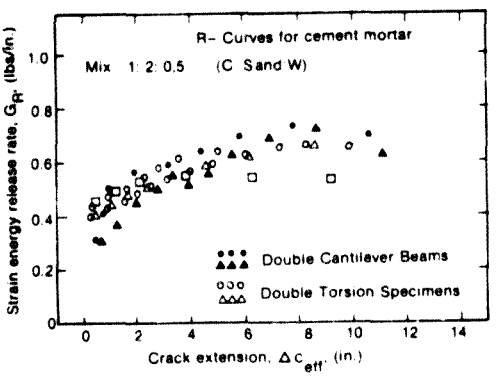

Figure 3.8 Specimen-type independent R-curves for cement mortar (from ref. 69)

Further summarised details of the work of Shah and co-workers follow:-

1. Extensive slow crack growth occurs in cemented materials. Using laboratory specimens with a single main crack, an extensive zone of microcracking also develops ahead of the visible crack tip. Aggregate interlock and pull-out occurs in this zone, (termed the "process zone"), which is the non-linear fracture zone in the specimen. This has led to the concept of two distinct crack depths:- the stress-free crack depth (c) in which crack surfaces are sufficiently displaced from one another to allow no stress interaction between them, and the effective crack depth (c_{eff}) which includes the stress-free crack and the non-linear zone ahead of the stress-free crack. If the size of this non-linear zone is termed z_{nl}, then:-

$$c_{eff} = c + z_{nl} \qquad (3.25)$$

Within z_{nl}, a stress distribution occurs equivalent to the crack-closing pressure, and is dependent at any point on the separation between the effective crack faces. At the point where the closing stress is zero, a characteristic separation occurs between the crack faces, termed the critical crack-tip displacement (or critical crack opening displacement COD). The crack will extend when this critical value is equalled or exceeded at the tip of the crack. The above concepts are illustrated in figure 3.9.

These authors found that z_{nl} was a function of specimen type and geometry. For their double torsion specimens, z_{nl} was approximately 25mm while for the double cantilever beams z_{nl} was approximately 75mm, for cement mortar. However, the point is made that the magnitude of z_{nl} is critically dependent on the value of COD, and will increase as COD increases.

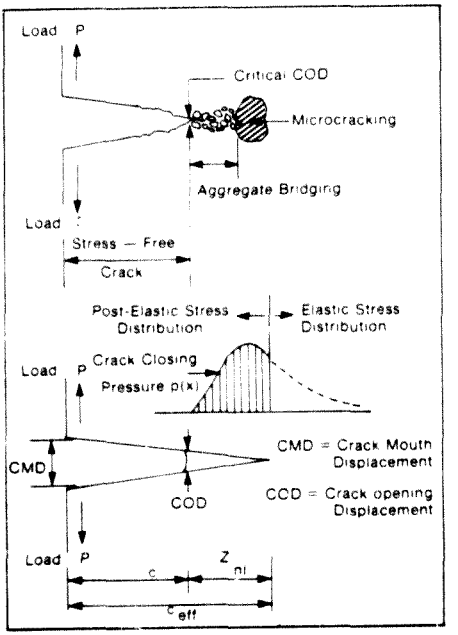

Figure 3.9 Illustration of concepts of effective crack depth and crack-closing pressure (from ref. 69)

2. Fracture resistance is measured in terms of a modified strain energy release rate term G_R. This term accounts for inelastic effects at the crack tip which lead to an additional component of energy characterised by the increase in permanent deflection of a specimen during a test. For load-cycling during a test when the load is progressively cycled between zero and a variable maximum value, the G_R term can be interpreted as the area enclosed by the load-deflection curve during a load-cycle. In this respect the G_R term is identical to the J' term introduced in 2.4. The authors have pointed out that without this modification of G_R, the effects of, for instance, aggregate addition are not apparent in the experimental R-curves.

The general conclusion of Shah et al was that R-curves can be used to characterise the resistance of cementitious materials during slow crack growth provided the ordinate value is modified to include for inelastic energy and the abscissa value is modified to account for the non-linear zone size. The concepts of their work were used and further extended in the experimental part of the present work.

The technique used to calculate R-curves for the present tests is elaborated in chapter 9.

3.5.2 J-INTEGRAL

The J-integral was first described by Rice[70], and has been proposed as a failure criterion for metals exhibiting elastic-plastic behaviour. Subsequently, researchers in the cemented materials field have investigated the use of J as a fracture criterion[35,36,37] in the hopes of overcoming some of the difficulties inherent in LEFM. The J-integral in its fundamental form is a path-independent energy line integral resulting from integration of strain energy density along a closed path around the crack. This fundamental definition is illustrated in figure 3.10. For a non-linear elastic body, J may be interpreted as the energy available for crack extension; for the linear case, J is equivalent to G.

In more practical terms, J may be considered as the potential energy difference between two identically loaded bodies having differing crack lengths. Drawing on a technique used in the metallic field, Mindess et al[35] evaluated the J-integral by testing cracked and companion uncracked specimens in order to compare their load-deflection curves. For their case of a beam in pure bending (third-point loading), the expression was:-

$$J = \frac{2}{bh}\int_0^{\delta_c} F \, d\delta_c \qquad (3.26)$$

where b = beam width

h = uncracked ligament depth

F = total load

δ = vertical displacement of the load point due to the crack only.

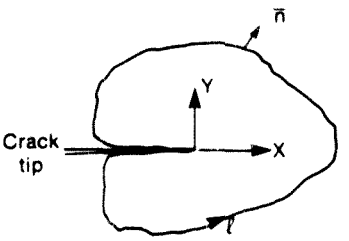

$$J = \oint_{\ell} W\,dy - \bar{T}.\left(\frac{d\bar{u}}{d\bar{x}}\right) ds$$

Where ℓ = Path of integration, taken counterclockwise around the crack tip;
W= Strain energy density;
$\bar{T}$= Traction vector defined by the outward normal vector $\bar{n}$ on the path ℓ;
$\bar{u}$= Displacement vector; and
s= Arc length along the path ℓ, $ds^2 = dx^2 + dy^2$.

Figure 3.10 Crack tip geometry and energy line integral (from ref. 36)

Hence, J is evaluated as the difference between the areas under the load-deflection curves of cracked and uncracked specimens. Strictly, these areas should be evaluated up to the point of crack initiation, but due to the difficulties of assessing sub-critical crack growth, this procedure is not always followed. Mindess et al[35] calculated J to the point of maximum load, as illustrated in figure 3.11. However, Mindess himself states:- "To be strictly valid, where deformation is not reversible, the J-integral refers

to crack initiation rather than crack propagation. Thus we can only look at the critical value of J at the point of crack initiation, J_{Ic}." It appears therefore that in this regard, J has the same fundamental limitation as K_c or G_c. A further difficulty in adopting J as a fracture criterion is the variability in determinations reported by investigators[28].

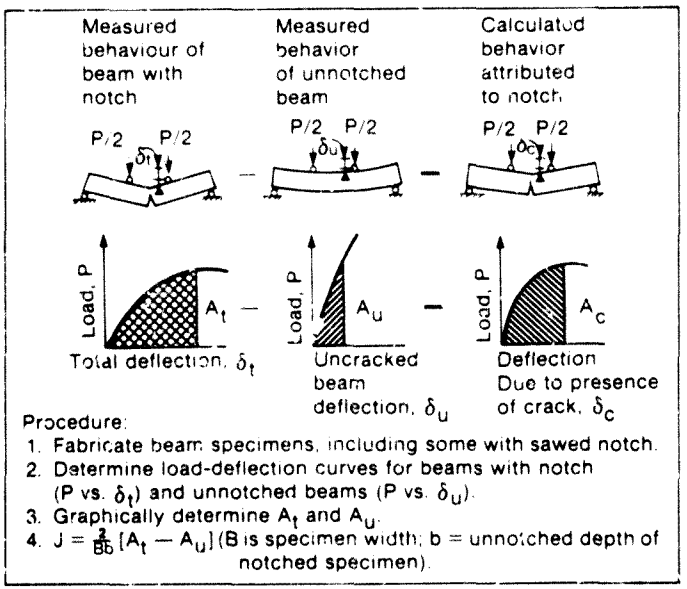

Figure 3.11 Experimental procedure to determine J (from ref. 36)

3.5.3 EFFECTIVE FRACTURE SURFACE ENERGY (WORK OF FRACTURE)

The work of fracture method can be used to give the effective fracture surface energy γ' of cemented materials. The formula used is:-

$$\gamma' = \frac{A_{F,\delta}}{A_f}$$

$$= \frac{A_{F,\delta}}{2A_0} \qquad (3.27)$$

where $A_{F,\delta}$ equals the area under the load-deflection curve, and A_f is the area of new fracture surfaces, conventionally taken as twice the cross-sectional area A_o. γ' is thus defined as the work done to create unit area of new fracture surface, ignoring irregularities on the fracture face. γ' is not necessarily the same at all stages in the fracture process.

It is important to point out that an evaluation of γ' for any particular test specimen is critically dependent on the measured area under, and hence the shape of, the load-deflection curve. This depends on aspects such as test machine stiffness and sensitivity response time of the recording devices. This is very much an instrumentation problem, since for those beams which fracture catastrophically when maximum load is reached, the transient effect of rapid crack growth and drop in load after failure is difficult to measure. Stable and semi-stable fractures can be created by notching, in which case a tail portion to the curve exists even when a nominally brittle material is tested. Unless the area under this tail portion is included in the term $A_{F,\delta}$, γ' may be substantially underestimated. The self-weight energy of the beam should also be included in the energy term, particularly for larger specimens. A component of self-weight energy after the machine load has dropped to zero also exists, and it is this energy which causes the remaining ligament in the specimen to be fractured by its self-weight.

γ' can be interpreted as the energy absorption of crack propagation, and equation (3.27) immediately relates it to both the surface free energy plus any other energy-absorbing processes that may be inseparably connected with fracture. In an ideal brittle material, the fracture surface area would equal twice the cross-sectional area of the specimen. However multiple microcracking occurs in the highly stressed zone of concrete specimens, as well as meandering

crack paths. Therefore the true fracture surface area may be many times larger than the effective surface area represented by the cross-sectional area. In the present work, a modified form of the parameter γ' is introduced which gives some measure of the true fracture surface area.

Blight[5] presumed that γ' comprised two components:- the true free surface energy of the material, and the plastic work component required to cause fracture. He included the following factors in the plastic work component:-

1. Work unaccounted for by the inability to accurately measure the true surface energy of the fracture surfaces.

2. Work done in dilatency and particle reorientation near failure.

3. Work done in producing microcracks that do not form part of the visible fracture surface.

4. Actual plastic deformation of the material.

Blight also suggested that the true fracture surface energy of a cemented material is represented by the surface energy of the cementing component. The effective fracture surface energy γ' thus exceeds the true surface energy γ by the amount of plastic work required to cause fracture. The engineer invariably requires γ' for his calculations, as long as γ' represents the failure mode likely to be experienced in practice. This means that testing procedures must be linked to actual service conditions for the material.

Another set of authors[63] have pointed out that the work of fracture method gives the effective fracture surface energy over the entire fracture process. Thus γ' will decrease with increasing notch depth as the fracture process becomes more controlled. Mai[71] has also used the effective fracture surface energy concept to analyse his tests on fibre-reinforced cements. Another development has been reported by Gurney and Hunt[72] who suggested a quasi-static method

of fracture toughness testing (basically a load-cycling method) where cracks can be made to grow in a controlled manner. They measured the work required to spread the crack per unit of nominal new crack area by means of a quantity R^*, as illustrated in figure 3.12. This method is similar to that of Shah and co-workers discussed previously[*1], except that the method of Gurney and Hunt does not account for inelastic effects (i.e. irrecoverable deformations).

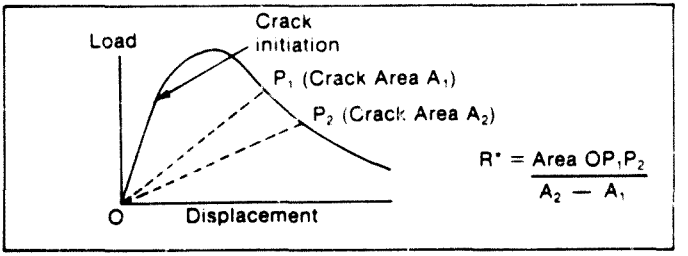

Figure 3.12 Principle of quasi-static method of fracture toughness testing (from ref. 72)

For perfectly elastic brittle materials (i.e. LEFM) there is an equivalence between γ' and G_c, viz:-

$$\gamma' = \frac{G_c}{2} \tag{3.28}$$

For this ideal case, γ' is also equivalent to the γ of the Griffith equation (2.2). At the critical point of unstable crack propagation, the Griffith equation assumes that the stored elastic energy is just sufficient to cause full failure of the specimen, i.e. the onset of crack growth is synonymous with fracture. Hence, the critical rate of release of strain energy with crack advance (G_c) becomes equivalent to the surface energy demand of new fracture faces. Needless to say, for non-ideal materials such as concrete, the above LEFM relations seldom apply. For this reason, γ' has been regarded as a NLFM parameter, since it accounts for the inelastic behaviour of cemented materials during fracture. A number of different γ' determinations have been made in the present tests, in

an attempt to identify their suitability to describe the fracture process.

It is interesting to note that a proposed standard test for the fracture of concrete based on the work of fracture method has been proposed by RILEM technical committee 50-FMC[73]. The test is designed to measure the fracture energy G_F, defined as the amount of energy necessary to create one unit of area of a crack (i.e. the same as $\mathcal{J}$). This test has been arrived at following the work by Hillerborg and others at the Lund Institute of Technology, Sweden, and appears to be an attempt to bypass the problems encountered in determining LEFM parameters on small specimens. Originally, Hillerborg[74] argued that concrete specimens with ligament depths of 1m and more would be required to obtain valid fracture parameters. However, the question of slow crack growth had been ignored in this assessment. Subsequently, Hillerborg has reverted to the use of small specimens for ease of handling and testing in the laboratory. However, the problem of small specimen size necessitated the use of a fracture parameter that was essentially non-linear.

According to the proposed RILEM test, beams of size 100x100x800 mm with an initial notch depth ratio of 0,5 are tested in three-point bending. Notches should preferably be sawn, and the number of specimens is increased as the maximum aggregate size increases. The specimen and notch sizes are intended to satisfy the conditions that the fracture should be stable and that damage is limited to a small zone along the ligament depth. Output from the test record should be the area under the load-deflection curve (W_0) the maximum deflection at final failure i.e. when the load on the machine drops to zero (δ_o), and the mean area of the initially uncracked ligament (A_{lig}). The fracture energy G_F is then evaluated as

$$G_F = \frac{W_0 + mg\delta_0}{A_{lig}} \qquad (3.29)$$

where mg is the total weight of the beam

Note that the γ' expression in equation (3.27) accounts for two new fracture surfaces, and hence G_F should be double the value of γ'. The term incorporating δ_o in the above expression is meant to allow for the fracture energy due to the self-weight of the beam. A simple analysis will show that, if δ_o is the beam deflection when the applied (machine) load drops to zero, the contribution of the self-weight to the fracture energy at this point is $mg\delta_o/2$. Therefore the self-weight term in (3.29) assumes that the deflection at zero machine load is one-half the ultimate deflection when total separation of fracture surfaces finally occurs. This assumption has been tested in the present work, and the G_F values of a number of specimens according to the RILEM proposal have been obtained (as γ' values). One further point should be mentioned: the test proposal states that it is acceptable to measure the deformation as the movement of the machine crosshead, although it is preferable to measure deflection relative to the support points. A proviso is added that if crosshead movement is measured, non-elastic deformations must have a negligible influence on the total measured energy. It would appear from the present and previous tests by the author [23] that localised crushing over the support rollers can account for up to 50 per cent of measured deflection, and the use of crosshead measurements is somewhat questionable. Finally, it should be mentioned that other proposals for a standard test method are being made, and the one by Jenq and Shah [9] might be referred to.

3.6 CONCLUDING REMARKS

The fracture mechanics parameters discussed above, while representing the majority of the common parameters that are available, are by no means an exhaustive list. A full discussion of all available parameters would be beyond the scope of this section. Suffice to say that other researchers have also presented techniques and parameters for characterising fracture in cemented materials, and reference might be made to the work of Bazant, and

Hillerborg and colleagues, reviewed by Mindess in ref. 28. Furthermore, Reinhardt[68] has presented an interesting approach to fracture, and his work has served as a basis for some of the analyses presented in this thesis. Finally, the work of Shah and colleagues[40,75] might also be mentioned. The fact that so many methods have been proposed indicates the complex nature of concrete fracture.

It is clear that as long as researchers are interested in the fracture phenomenon, and since the structure and behaviour of concrete are highly complex, there will be new approaches presented, argued over, accepted, modified or rejected. Unfortunately, not all these proposals will be able to be thoroughly tested. However, this interaction represents an essential part of the scientific method, and it is to be hoped that the concrete fracture field will develop to a point where, not only will test data be able to be properly analysed, but also measured parameters will be useful tools in advancing the analysis and design of concrete structures.

PART II EXPERIMENTAL FRACTURE WORK

The background to concrete fracture testing, based on a literature survey and presented in the previous part, has served to highlight aspects that require further study. Amongst these are fracture processes in notched concrete beams, including the presence, extent, and influence of microcracking; the effects of specimen depth and notch depth on fracture; and the evaluation of fracture parameters in the light of these aspects. An experimental programme was therefore designed to address these questions. Three series of tests spanning a period of three years were carried out on notched concrete beams of variable sections and depths. Test apparatus and instrumentation were designed, constructed and assembled. Chapter 4 will describe details of specimens, mixes and materials, test equipment and testing procedures. Chapter 5 will deal with results for materials control tests, and certain basic aspects of the fracture test results such as notch-sensitivity of fracture beams, the influence of support roller friction on loads and deflections, and characteristic shapes of load-deflection curves.

4 TESTING OF FRACTURE BEAMS

4.1 INTRODUCTION AND OBJECTIVES

An MSc(Eng) dissertation (1974) by the author[21] examined the problem of plane strain fracture testing of cemented construction materials. In that work the aim was to study the fracture mechanisms of a portland cement mortar and apply the results to the development of tentative criteria for fracture testing. It was recognised that an understanding of fracture mechanisms and their influencing factors is the first step towards applying fracture tests in the development of new and improved materials, and towards applying fracture principles in design and analysis. The effects of specimen dimensions, testing machine stiffness, and rate of loading on the LEFM parameters K_c, G_c, and on the NLFM parameter δ', were studied. It was found that all these variables profoundly influenced the measured fracture toughness as well as the post-cracking behaviour of the notched beams. The results for the MSc(Eng) work are briefly summarised below.

4.1.1 EFFECT OF SPECIMEN GEOMETRY ON LEFM PARAMETERS

NOTCH DEPTH RATIO

Fracture toughness of unnotched beams were considerably higher than those of notched beams, and a basic difference existed between the

modes of fracture of these two types of specimen. This difference was related to the amount of st .n energy stored in the specimen at the point of fracture, and to the volume of highly stressed material in which energy-absorbing mechanisms could operate, both of which were greater in the case of the unnotched beams. This was also borne out by the fact that strain rate had a more marked effect on the failure load of unnotched beams, since at low strain rates a greater degree of stable microcrack growth from the surface of the beam could occur than at higher strain rates. For a notched beam, the critical crack initiated at the notched section and microcracking was limited to this section.

BREADTH/DEPTH (b/d) RATIO

While it appeared that narrow beams (b/d = 0,5) gave higher fracture toughnesses than flat slabs (b/d > 2), the effect of absolute specimen epth tended to obscure the results, since it was also the deeper sections that gave the higher toughnesses. It would appear from the results that plane strain conditions predominate in the testing of cemented materials, and that the effect of absolute depth is more important than that of b/d ratio. Nevertheless, this effect of plane stress/plane strain was recognised as requiring further experimental study.

4.1.2 EFFECT OF STRAIN RATE

This variable was shown to have an important influence on measured load-deflection curves and on fracture parameters. Failure to control the strain rate at consistent values during tests led to excessive var' bility and scatter of results, mainly due to the creep component of deflection. It was found that failure compliances of beams could more than double when very slow strain rates were used, while the corresponding effect on a parameter such as K_c was to reduce its value by about 25 per cent. Provided the

strain rate, measured in terms of deflection of the load points, exceeded 1 um/s, the measured fracture parameters could be considered to be independent of the deflection rate. This aspect has application in fracture testing of materials to be used in situations where deformations and loadings are time-dependent, such as road pavements.

4.1.3 EFFECT OF TEST MACHINE STIFFNESS

Post-cracking behaviour was profoundly affected by the stiffness of the loading system, and unrepresentative load-deflection curves were obtained when the system could feed energy back into a specimen at the critical point of unstable crack propagation. The importance of a stiff test set-up was therefore clearly recognised.

This previous experimental work allowed tentative test criteria for cemented materials to be suggested. The most important involved specimen size requirements. Fracture toughness calculations are based on a mathematical model of the stress/strain field ahead of a crack tip, and the reliability of the calculated parameters depends on the accuracy of the model. Provided the size of the inelastic zone is small in relation to specimen dimensions, the concepts of LEFM can be applied. To evaluate this, a pseudo-plastic zone size parameter R' was defined, which is analogous to the parameter R which measures the size of the plastic zone in metallic specimens. Limiting values of ratios involving R' were suggested as being necessary to ensure that valid fracture parameters were measured. It was also suggested that a fracture specimen should fail in a stable or semi-stable fashion if valid lower-limit parameters were to be obtained. This implied that notched specimens ought to be used While notching was necessary, initial notch depth ratios equalling or exceeding about 0,5 were undesirable since no true spontaneous crack propagation occurred and large errors were introduced into the fracture calculations. Referring to

the requirement of stable or semi-stable fracture it was important that the balance between the energy stored in the loading system and the strain energy in the specimen at the point of failure be considered, since this balance governed the interaction between loading system and specimen during crack propagation. If energy could be fed back into the specimen, an unrepresentative load-deflection curve was obtained and catastrophic fracture could result.

Part of the MSc(Eng) work involved use of a load-cycling technique to obtain stable crack growth. This technique, in which the beam was loaded until the critical point of fracture instability was approached and the load then rapidly removed before instability could occur, allowed a crack to be extended in stable increments through the beam until final failure. With each successive load cycle, there was an increase in compliance and permanent set; resistance to crack closing and re-opening was also present. What was especially significant in the load-deflection record was that each reloading cycle gave a markedly linear portion of the curve, indicating an elastic-type deformation during the early stages of loading when the crack was accommodated within elastic surroundings.

To summarise, the MSc(Eng) investigations identified and isolated those test variables which significantly affected measured fracture parameters. Two LEFM parameters were evaluated (K_c, G_c) as well as the NLFM parameter of effective fracture surface energy (γ'), using tests on notched beams. Geometrical and dimensional ratios, strain rates, and testing machine stiffness influenced the results. Notched beams had lower fracture toughnesses than unnotched beams. It was recognised that the questions of absolute specimen size and the plane stress/plane strain effect required further investigation. Nevertheless, the general conclusion was that the concepts of strain energy release rate and fracture toughness were applicable to cemented materials. However, non-linear and extensive post-cracking behaviour gave to these materials a quasi-ductile fracture that would require modifications to the basic fracture formulations.

The present experiments were designed with this previous work as background, but also drawing upon the progress that had been made in the field of elastic-plastic fracture. It was obvious that the application of these new principles to cemented materials should be tested. Nevertheless, the LEFM formulations were also retained in view of the testing of very large fracture specimens to which they might conceivably apply. The overall framework within which fracture studies on cemented materials are carried out should always be kept clearly in view if meaningful results are to be obtained. This framework comprises, inter alia, the development of a design methodology based on fracture mechanics principles, the establishment of criteria and procedures for valid fracture testing, the study of fracture processes and mechanisms, and material characterisation. With these observations in mind, it was possible to define specific objectives for the present fracture testing programme. These objectives were:-

1. To extend previous work done at the University of the Witwatersrand by the author[23] and others[76,77] on the fracture properties of concretes. The work done at Wits has centred on macroscopic fracture behaviour in the sense that fracture of concrete and cemented materials has been studied on normal laboratory sized specimens and the material has been considered as a composite.

2. To investigate fracture processes by careful study, characterisation and analysis of load-deflection curves obtained during fracture tests. Other experimental techniques of strain and ultrasonic pulse velocity measurements were also used to study fracture processes.

3. To investigate the effect of specimen size on linear elastic (LEFM) and non-linear (NLFM) fracture mechanics parameters. To this end concrete beams covering a range of depths from 100mm to 800mm, spans from 400mm to 1200mm, and ligament depths from

50mm to 640mm, were cast and tested in order to evaluate fracture behaviour.

4.2 DETAILS OF SPECIMENS

Two series of fracture tests on concrete specimens of varying sizes and shapes were conducted during 1982, and a further series during 1985. Series F1 comprised prismatic constant section beams with major support spans varying from 400mm to 2000mm, and depths from 100mm to 500mm respectively. In all cases a constant span/depth ratio of four and beam width of 100mm were used. Series F2 comprised firstly prismatic constant section beams with span/depth ratio of either four or eight, but with constant overall depth of 100mm; secondly large beams of span 3200mm and depth 800mm were tested, and these beams were triangular in elevation with variable sections to reduce their mass. Series F3 comprised both constant and variable section beams with a ratio of span/depth at mid-span of four. Beam depths varied from 100mm to 500mm, and the 300mm and 500mm deep beams had a variable section to reduce mass. Small vertical "steps" were cast on the sloping faces of these beams to accommodate ultrasonic test probes. "Demec" strain targets at mid-span and covering the beam depth were fixed to one side of all beams on a 100mm gauge length. Cast-in central notches with notch depth ratios of 0,2, 0,25, 0,4 or 0,5 were used. Four 100mm deep beams of series F3 had notches cut by a diamond-tipped saw-blade. A summary of the various specimens is given in table 4.1, in which it can be seen that a total of 69 fracture beams were tested. Figure 4.1 shows details of the constant and variable section beams. Figures 4.2(a) and (b) show photographs of large variable section beams immediately before being placed on a test bed. (Note the vertical "steps" on the beam in figure 4.2(b)).

For all series, control cubes (101,6mm) for compressive strength were cast. For series F1 control unnotched beams (101,6x101,6x610mm)for modulus of rupture and flexural elastic

Table 4.1 Summary of fracture beams, Series F1, F2 and F3

Series	Specimen number	Overall beam dimensions (mm) bxdxL	Initial notch depth ratio c_o/d	Loading span (mm) S	Initial ligament depth (mm) h_o	Number of beams
F1 (cast and tested during June, July, August 1982)	F1/1,2	100x500x2100	0,2	2000	400	2
	F1/3,4	100x500x2100	0,4	2000	300	2
	F1/5,6	100x300x1200	0,2	1200	240	2
	F1/7,8	100x200x800	0,4	800	120	2
	F1/9,10,11	100x100x400	0,25	400	75	3
	F1/12,13,14	100x100x400	0,40	400	60	3
1. All F1 beams had constant sections.				Sub-Total F1		14
2. Beams with L=S in above table were tested on loading spans slightly less than those given above, the difference however never exceeding 2,5%. This nominal change to the loading span was not considered to have materially affected the fracture data.						
F2 (cast and tested during October, November 1982)	F2/1	100x800x3400	0,2	3200	640	1
	F2/2,3,4	100x800x3400	0,4	3200	480	3
	F2/5 - 8	100x100x450	0,25	400	75	4
	F2/ ,	100x100x450	0,4	400	60	7
	F2/16 - 26	100x100x850	0,5	800	50	11
1. Beams F2/1 - 4 had variable sections. Beams F2/5 - 26 had constant sections.				Sub-Total F2		26

Table 4.1 (Continued)

Series	Specimen number	Overall beam dimensions (mm) bxdxL	Initial notch depth ratio c_o/d	Loading span (mm) S	Initial ligament depth (mm) h_o	Number of beams
F3 (cast and tested during March, April, May 1985)	F3/1,2	100x500x2125	0,2	2000	400	2
	F3/3,4	100x500x2125	0,4	2000	300	2
	F3/5,6	100x300x1275	0,2	1200	240	2
	F3/7,8,9	100x300x1275	0,25	1200	225	3
	F3/10,11,12	100x300x1275	0,4	1200	180	3
	F3/13,14	100x200x850	0,2	800	160	2
	F3/15,16	100x200x850	0,4	800	120	2
	F3/17 - 23	100x100x450	0,2	400	80	7
	F3/24	100x100x450	0,25	400	75	1
	F3/25 - 29	100x100x450	0,4	400	60	5

1. Beams F3/1 - 12 had variable sections.

2. Beams F3/13 - 29 had constant sections.

3. Beams F3/21 - 23 and F3/29 had sawn notches.

Sub-Total F3	29
Total F1, F2 & F3	69

4. One beam (200/0,2) was fractured by accidental overdrive of the test machine. No results obtained.

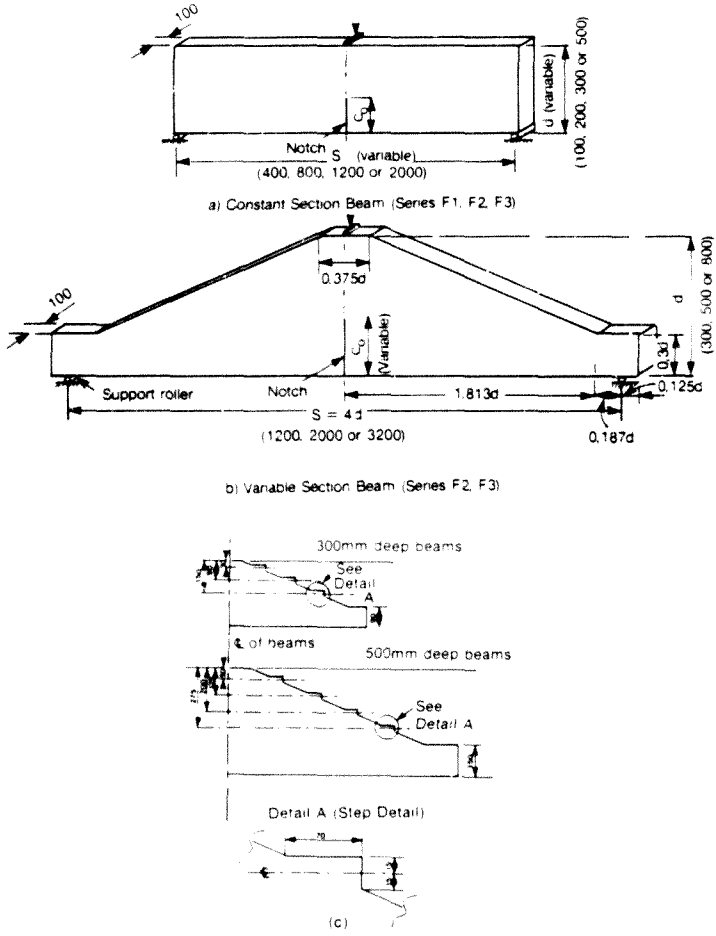

Figure 4.1 Details of constant and variable section notched beams (a) Constant section beams (b) Variable section beams (c) Details of "steps" on sloping faces of variable section beams



Figure 4.2(a) View of 800mm deep variable section beam being manoeuvred onto test bed (series F2)

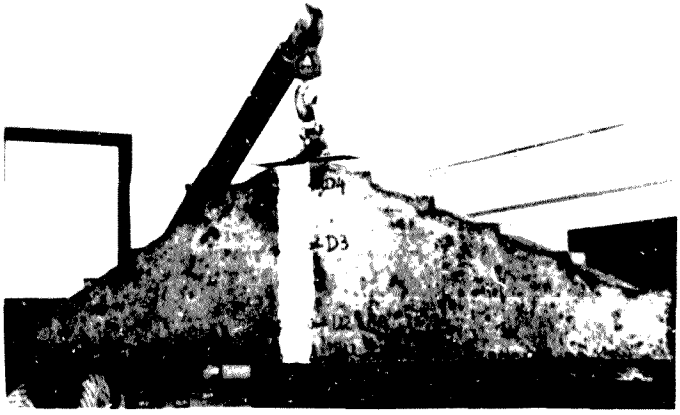

Figure 4.2(b) View of 500mm deep variable section beam being manoeuvred onto test bed (series F3)

modulus values were cast, while for series F2 control prisms (100x100x200mm) for compressive elastic modulus were cast. Series F3 had control prisms (100x100x200mm) for compressive elastic modulus, and control beams (100x100x400mm) for modulus of rupture (MR) tests. A number of these control beams were unnotched to obtain conventional MR values, while others were notched to varying initial depths in order to investigate notch-sensitivity of the material. For all three series, a total of 162 control specimens were cast and tested to provide basic material properties.

4.2.1 SPECIMEN IDENTIFICATION

For clarity, fracture specimens are identified according to the following system:-
F series/beam no.(depth/initial notch depth ratio) where "F" refers to fracture tests, "series" refers to series number, "beam no." and "initial notch depth ratio" are as given in table 4.1 and "depth" refers to the depth of the beam in millimetres. Thus, for example, series 3, beam number 1 was 500mm deep with an initial notch depth ratio of 0,2; it is referred to as F3/1(500/0,2).

4.3 CONCRETE MIXES

The mix proportions used for the tests are shown in table 4.2. Details of the materials, mixing, casting and curing are given in appendix A. From table 4.2, mix ratios by mass were:-
1:0,53:2,07:2,80 (cement:water:sand:stone).

Slumps for series F1 and F2 varied from 30 to 60mm, and for series F3 from 80 to 130mm. (See 5.2.3 and appendix C for discussion on effect of slump on material properties).

Table 4.2 Concrete mix proportions for fracture tests

	Materials	Mix proportions in kg/m³, (Dry materials)
Cement:	Ordinary Portland	375
Stone:	Crushed 19mm nominal single-sized	1050
Series	F1 and F3: Reef quartzite	
Series	F2: Reef quartzite and Halfway House granite	
Sand:	Reef quartzite crusher sand	775
Water:	Potable tap water	205

4.4 TEST EQUIPMENT

Instrumentation for the tests involved the use of a load cell and LVDT transducers to measure mid-span load and deflection. Various recorders received the load cell and transducer outputs and autographically plotted the results. The primary output from the tests was load-deflection plots. However, tests for series F3 included assessment of crack growth and size of non-linear zone ahead of the main crack, by means of ultrasonic pulse measurements, strain measurements across the fracturing section, and visual observation of crack depths. The majority of tests for series F1 and F2 had simple monotonically increasing deflections during the tests, with the load rising to a maximum and then gradually dropping to zero as the beam continued to deflect. (Note:- since the testing ma-

chines were very stiff compared to the specimens, the tests were effectively deflection controlled). Most of the tests for series F3 used a load-cycling technique described earlier in 4.1, and a small number of tests for series F1 and F2 also used this technique.

The apparatus and recording equipment will be described first, followed by details of the testing procedure primarily for series F3 since these tests were more complex than those of series F1 and F2.

4.4.1 DEFLECTION - MEASURING RIG

Mid-span beam deflections were measured using a number of different arrangements depending on the size and shape of the specimen. Extraneous deflections were excluded from the measurements since it had been found earlier[23] that these could seriously affect the accuracy of the results. A basic deflection rig and specimen clamp were designed, and the rig was adjustable so as to accommodate all the constant section beams. With modification it could also be used for the variable section beams. The rig was supported on the horizontal upper face of the beam over the two end supports thus eliminating the recording of deflections due to localised crushing over the support rollers. Mid-span deflection under the loading roller was measured using a device that clamped onto the specimen at a distance of either 10mm or 20mm below the roller. The two screw-clamp portions of this device supported the moving cores of two linear variable differential transformers (LVDTs), the barrels of which were clamped in the deflection rig. Photographs showing the rig and clamp are shown in figures 4.3 (a) to (d). Features to note are the load cell, the LVDTs, the loading roller with centralised steel ball, a knife-point support for the deflection rig. Details of the rig are given in appendix B.

Extraneous deflections due to localised stress and strain concentrations under the loading roller were also investigated. The

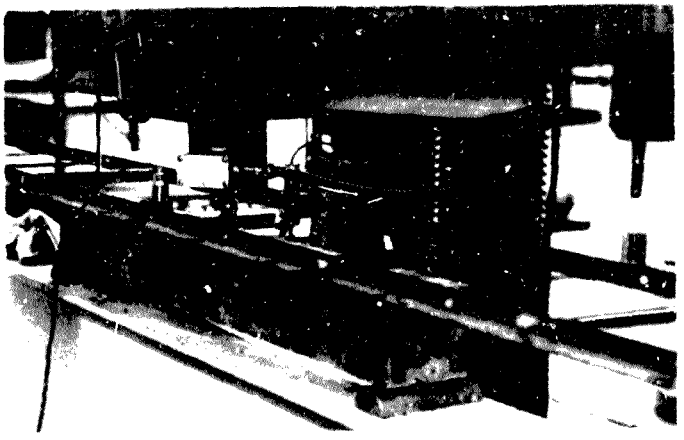

Figure 4.3(a) Deflection rig and specimen clamp in use on a 1x1000x8000mm beam (Series F2)

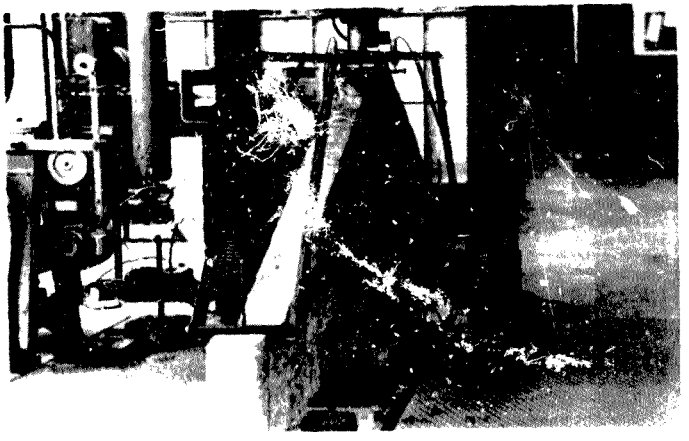

Figure 4.3(b) Modified deflection rig in use on a 1000x800x3200mm beam (Series F2)

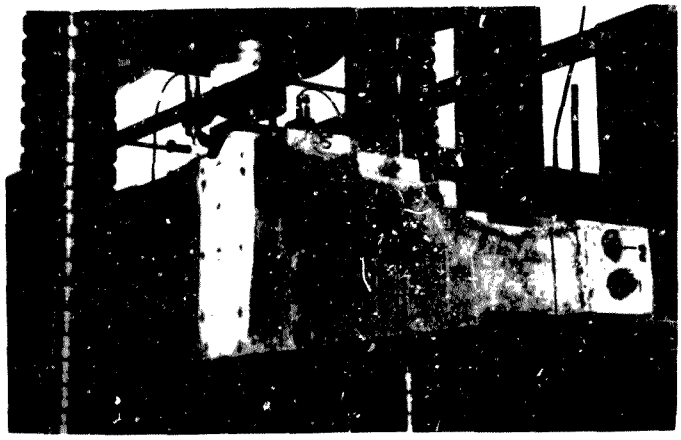

Figure 4.3(c) Modified deflection rig in use on a 100x3 0x1.0mm beam (series F3)

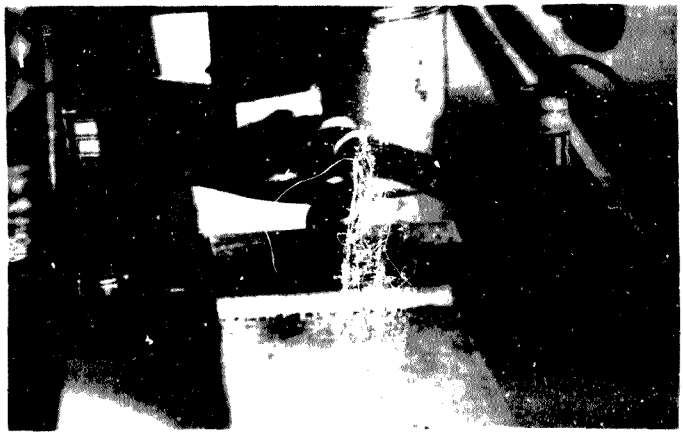

Figure 4.3(d) Details of specimen clamp and LVDTs

magnitude of these deflections was a maximum of about 10 per cent of the total deflection measured at maximum load. An analysis of the effect on compliance and fracture parameters showed that errors of about 10 per cent might be induced in the former, but only about 5 per cent in the latter. It was impossible to assess these deflections for every beam. Since the error induced in estimating slow crack growth from compliance measurements would be greater than the error associated with these deflections, this effect was not included in analyses, particularly since calculated parameters were so little affected. Measurements such as areas under load-deflection curves would be affected hardly at all since the load returned to zero at the end of the test. Details of measurements of these extraneous deflections are given in appendix B.

4.4.2 ELECTRONIC TRANSDUCERS

LOAD CELL

This was used for all tests except beams F3/17-20 and F3/24-26. The cell had a capacity of 20kN, and was calibrated using the Amsler testing machine (see later) and a digital millivoltmeter, or directly onto the recorders. (See appendix B for further details of the load cell).

LINEAR VARIABLE DIFFERENTIAL TRANSFORMERS (LVDTs)

The deflection rig supported two LVDTs, one on either side of the specimen, in order to obtain the mean deflection. The outputs of the LVDTs were electrically averaged before being fed to the recorders.

The LVDT cores were attached to the arms of the specimen clamp using plasticised modelling clay. Calibration was carried out by connecting the LVDTs in parallel, and mounting them on a small bed in

which a micrometer gauge was used to vary the deflection. A number of calibrations was carried out using a millivoltmeter or directly onto the recorders. (See appendix B for further details of the LVDTs.)

4.4.3 RECORDING EQUIPMENT

Three types of autographic load and deflection recording equipment were used.

XY RECORDER

This recorder had an effective plotting area of 360mm (X scale) x 240mm (Y scale). (Two independent Y channels were available). It had been found previously[23] that a fracture beam experiencing rapid crack propagation produced a load-deflection trace that could not be adequately followed by an XY recorder due to the relatively large inertia of its moving parts. This was also true for the present recorder, but fortunately all the beams except a single 800mm deep beam fractured in a stable or semi-stable fashion and the post-peak portion of the curve could be recorded. It was also important to record the extreme tail portion of the curve, and in particular that portion when machine load was no longer being applied to the beam and the beam was failing under its own weight. The energy for this final portion of fracture is a significant component of the total fracture energy. The XY recorder was unable to record this portion and a further recorder was used as detailed below.

STRIP CHART RECORDERS

TWO-PEN RECORDER

Output from most of the tests of series F1 and F2 was also fed to this recorder to measure the zero-load extreme tail portion of the curve, and to check the XY record. The recorder had two moving pens with a faster response time than the pens of the XY recorder, and which recorded load and deflection on a moving paper chart which could be driven at various speeds. As will be shown later in chapter 5, maximum pen speeds were insufficient to record beam deflections at or near ultimate fracture accurately and therefore a different recorder was used for series F3.

MULTI-CHANNEL RECORDER

Output from series F3 tests was fed to this recorder in addition to the XY recorder. Preliminary tests to determine pen speeds of the recorder showed that it could adequately measure the extreme tail portions of the load-deflection curves. (See later 5.5). The paper chart was normally driven at 10mm/min or 25mm/min, but the speed was increased to 10mm/s or 25mm/s for the final portion of the record approaching ultimate failure.

See appendix B for further details of recorders and power modules.

ULTRASONIC PULSE EQUIPMENT

The tests of series F3 incorporated an ultrasonic pulse recorder in an attempt to monitor the progress of cracking and damage as the crack grew through the beam. The recorder comprised transmitting and receiving probes linked to a central control unit which automatically measured the pulse transit time between probes and displayed it on a digital meter. Preliminary tests showed that the transit time of a pulse emitted at 40kHz was sensitive to crack growth and non-linear zone extension if the pulse was transmitted longitudinally through the beam, but insensitive if the pulse was transmitted across the width of the beam at mid-span. For this reason, the variable section beams of series F3 had vertical "steps" cast on the sloping faces to accommodate the probes at various heights above the lower face. For the constant section beams, the

probes were placed at various heights on their vertical end faces. In this way, the progress of cracking could be monitored by noting the increase of the transit time at any particular position as the test progressed. Figure 4.4 shows the positions for ultrasonic measurements for the beams of series F3. Appendix B contains further details of the ultrasonic equipment.

STRAIN EQUIPMENT

In order to estimate non-linear zone size, strains in the intact region of the beam ahead of the main crack tip as well as crack width were measured during series F3 tests. Four pairs of "Demec" strain targets at mid-span and covering the beam height were fixed to one side of all F3 beams. The targets were positioned such that pairs 1 and 2 coincided with the lower edge and tip of the pre-formed notch respectively, while pairs 3 and 4 coincided roughly with the initial position of the neutral axis and a point initially within the compression zone of the beam respectively. Two strain gauge instruments with 100mm and 200mm gauge lengths were used. The 100mm gauge was used for the lower three sets of readings on each beam, while the 200mm gauge was occasionally used for the upper set of readings where the dial of the smaller gauge tended to interfere with the deflection clamp. Details of the heights in millimetres above the lower edge of a beam at which strains were measured are given in the list below:-

(c_0/d = initial notch depth ratio)

Beam depth 100mm:-	10	$100c_0/d$	60	80
Beam depth 200mm:-	10	$200c_0/d$	120	180
Beam depth 300mm:- c_0/d=0,2	10	60	150	250
Beam depth 300mm:- c_0/d=0,25	10	$300c_0/d$	180	245
or 0,4				(or 265)
Beam depth 500mm:- c_0/d=0,2	10	100	300	445
Beam depth 500mm:- c_0/d=0,4	10	200	350	445

It was assumed that the strain readings represented average strain across the gauge length before the crack had traversed the gauge

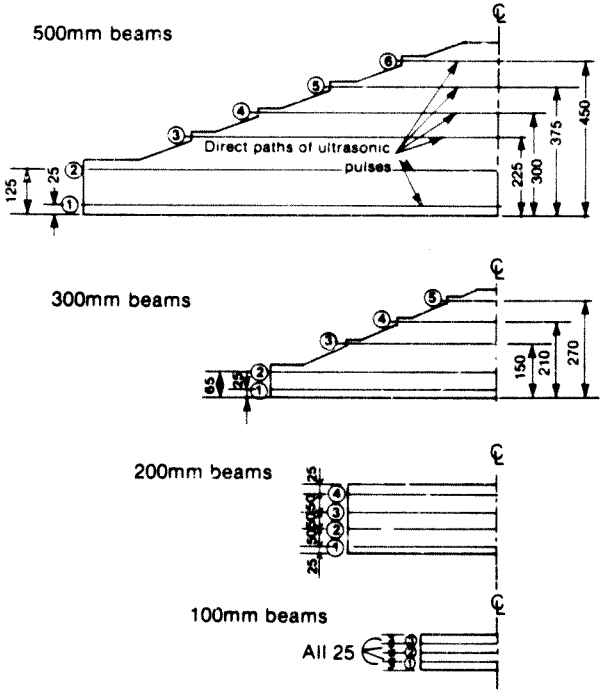

NOTE: Only one-half of beams shown, due to symmetry.
Ultrasonic pulses were transmitted longitudinally (i.e. horizontally) from one end of the beam to the other.

Figure 4.4 Positions for ultrasonic measurements (series F3)

position, and crack width after the crack had passed the gauge position. These two assumptions are reasonable; in particular, deformation across a cracked section can be assumed to be concentrated in the crack with the zones on either side of the crack being effectively destressed. Appendix B contains details of the strain equipment.

4.4.4 TESTING MACHINES

Three hydraulic testing machines were used. The machine for series F1 and most of series F3 was an Amsler type 103 compression machine which was manually operated and had a maximum capacity of 2000kN. Specimen loads were measured by the load cell which was clamped to the upper machine platen. The machine could accommodate beams up to 2000mm span on a stiff beam bed. The beams for series F1 were supported on the beam bed using 50mm diameter half-round steel rollers, which ran on hardened steel cylinder-bearing races. Spreading of beam ends was thus allowed. For series F3, the beams were supported on the beam bed rollers, which were generally free to move laterally (see later section 5.5). Figure 4.3(c) shows a test set-up of the Amsler machine with a 300mm variable section beam in position.

The machine for series F2 was a Macklow-Smith compression testing machine, manually operated, of maximum capacity 1750 kN. This machine could accommodate up to a 3500mm long beam on a very stiff beam bed situated in a floor well. The load cell was fixed to the top platen. The small fracture beams of this series were supported on the roller/bearing supports described above, but the large variable section beams were supported on the beam bed rollers. These rollers could be released immediately prior to a test, thus allowing spreading of beam ends. Figures 4.3(a) and (b) show details of the arrangement for series F2.

Seven of the 100mm deep beams of series F3 (beams F3/17-20 and 24-26) were tested in a Tinius-Olsen universal testing machine with a capacity of 600kN. These beams were supported on the beam-bed through rollers contained in concave supports, thus preventing the spread of the beams. It was possible to use the electronic load output from the machine, thus eliminating the load cell. Figure 4.5 shows the arrangement for these beams. Note the roller support and the "demec" strain targets.

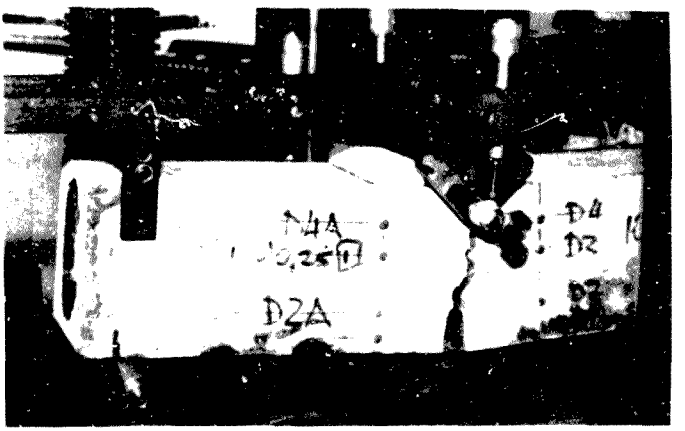

Figure 4.5 Detailed view of small fracture beam in Tinius-Olsen machine (series F3)

The importance of a stiff test arrangement in fracture testing of cemented materials has long been recognised[23]. A stiff arrangement limits the amount of elastic energy (strain energy) stored in the machine and load-carrying elements at fracture initiation. Part of the reason for notching a specimen is to achieve a similar effect of limiting the strain energy in the specimen. By paying attention to these aspects of machine stiffness and specimen notch geometry, it is possible to produce a crack that propagates in a stable fashion throughout the test, and this simplifies obtaining a complete test record. By using fairly stiff testing machines for the present tests, and by limiting the total specimen load to about 1

per cent of machine capacity, it was possible in all but one case to obtain complete test records (i.e. stable to semi-stable fractures).

4.5 TEST PROCEDURE

The procedure described below applies primarily to the fracture tests of series F3 which used a load-cycling technique. However, the principles of the procedure also applied to series F1 and F2 where monotonically-increasing deflection was generally used in the tests. Ultrasonic pulse and strain measurements, and visual estimate of crack depth, were only made during series F3 tests.

4.5.1 SPECIMEN PREPARATION

All beams were damp-cured, generally under moist hessian and plastic sheeting (see appendix A for details). About 24 hours before testing, beams with section depths greater than 100mm were raised off their casting beds into a vertical position, taking care not to cause tensile stresses at the notch root. Strain targets were glued to one vertical side of the beam, symmetrically about the mid-span. An area approximately 100mm wide about the mid-span on both vertical faces was painted with white PVA paint, to allow observation of visible crack growth. During casting, these surfaces had been made smooth using perspex sheets. The specimens were then covered again with damp hessian and plastic sheeting until the test. All specimens were saturated at the time of test. Beams were placed on the machine bed for testing, if necessary using a small mobile crane and hooks locating in cast-in lifting rods (see figure 4.2(b)). After positioning the specimen clamp, loading roller, and deflection rig, the LVDTs were zeroed and a thin layer of petroleum jelly applied to the surfaces where the ultrasonic probes were to

be placed. Initial readings of ultrasonic pulse transit time and strain gauge divisions were taken. In most cases the beam support rollers were then released to allow spreading of the beam ends during the test.

4.5.2 LOADING

A load-cycling technique to create stable crack growth was used as follows:-

1. Generally one to two cycles were applied before maximum load, followed by between six to eight cycles after maximum load.

2. On any particular cycle, the deflection at maximum load was maintained as far as possible without inducing additional deflection, to allow strain readings to be taken. Maintaining this deflection was not easy, particularly near the maximum load portions of the record, since stable slow crack growth tended to occur. If crack growth as observed by the movement of the XY recorder pen threatened to become unstable (in the sense of rapid crack growth), a small amount of load was rapidly "dumped" before attempting the strain readings. For the shallow notched beams in particular, the record invariably showed some load reduction (of the order of up to 20 per cent of the cycle's maximum load) accompanied by a limited increase in deflection (see later figure 4.6). In addition to strain readings taken at or near maximum cycle load, the depth of the visible crack was observed by very careful examination of the beam surface with the naked eye, and the position of the crack tip marked on the beam on both opposite vertical faces On occasions, strain readings were also taken at the end of a cycle.

3. Ultrasonic pulse transit times were measured after unloading on any particular cycle. Preliminary trials had shown that the pulse time was relatively insensitive to whether measurements

were taken at maximum load during a cycle or at zero load after a cycle.

4. For the final test cycle, when the crack was usually very close to the upper surface of the beam, the beam was loaded at a uniform rate of deflection until ultimate fracture. This was represented by the rapid falling of the two fractured portions. As ultimate fracture was approached, the chart speed on the multi-channel recorder was increased to produce an accurate record of ultimate fracture.

5. After the test the fractured faces of the beam were inspected for any unusual features, and the depths of the cracks for the various load cycles were measured on both faces.

A typical test therefore produced two independent load-deflection records as well as (for series F3) strain/crack width readings, ultrasonic pulse measurements, and depths of visible cracks. This basic data was analysed to produce crack growth and compliance data, fracture energies, and other fracture parameters. For a non load-cycled test, continuous load-deflection curves were available.

The points described above are best illustrated with reference to portions of an actual test record, shown in figures 4.6(a) and (b) for the XY and multi-channel recorder respectively. The relevant beam is F3/15(200/0,4).

FIGURE 4.6(a)

The first three and a half cycles of the test are shown in this figure. Note the following:-

1. Two cycles were achieved before maximum load. The peak for cycle 1 shows that some stable crack growth occurred while the strain readings were being taken at this point.

2. On the [illegible] load cycle (cycle 2) loading was stopped at the apex of the cycle. This was immediately followed by an increase in deflection accompanied by load reduction due to the unstable nature of crack growth near maximum load. Hence, the descending portion of the curve at this point may be regarded as stable spontaneous crack growth. On occasions, the maximum load point would be followed by rapid crack growth leading to a large increase in deflection and reduction in load. This condition was regarded as unstable spontaneous crack growth.

In order to arrest the stable spontaneous crack growth following maximum load, it was necessary to rapidly unload the beam from point A to point B, where strain readings could be taken before unloading.

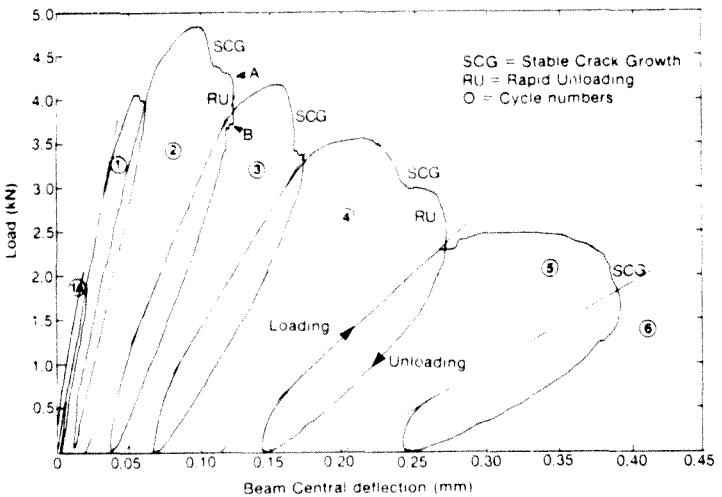

Figure 4.6(a) Portion of XY test record for beam F3/15(200/0,

3. Similar features as noted for cycle 2 can by seen for cycle 3. However, the tendency for spontaneous crack growth reduced as the test progressed.

4. Permanent plastic set δ_p occurred at the end of each load cycle. This irrecoverable deformation increased as the test progressed, and was due to resistance to crack closing brought about by fragmentation behind the crack tip and crack bridging by dislodged and wedged aggregate particles. The irrecoverable deformation profoundly influenced the assessment of beam compliances and fracture energies, as will be shown later.

5. On cycle 6, the sensitivity of the X scale was halved.

FIGURE 4.6(b)

This shows the multi-channel record corresponding to the XY record of figure 4.6(a). Note the following:-

1. The various load cycles can be clearly seen. The deflection record experienced very little displacement at this stage, since the sensitivity for this record was set such that the much larger deflections at or near ultimate fracture could be measured.

2. The load record for cycle 2 clearly shows load reduction under spontaneous crack growth followed by rapid unloading.

3. The periods of zero load represent the time during which ultrasonic readings were taken.

4. A portion of the record for beam F3/1(500/0,2) is shown as an inset in figure 4.6(b) to illustrate more clearly the effect of unstable spontaneous crack growth which is very rapid, as shown by the nearly vertical lines in the inset.

A final illustration from the tests, given in figure 4.7, is a photograph of the face of a 500mm deep beam (F3/1(500/0,2)) showing the progress of the main crack with the numbers of the load cycles marked on the beam. The initial starter notch can also be clearly seen.

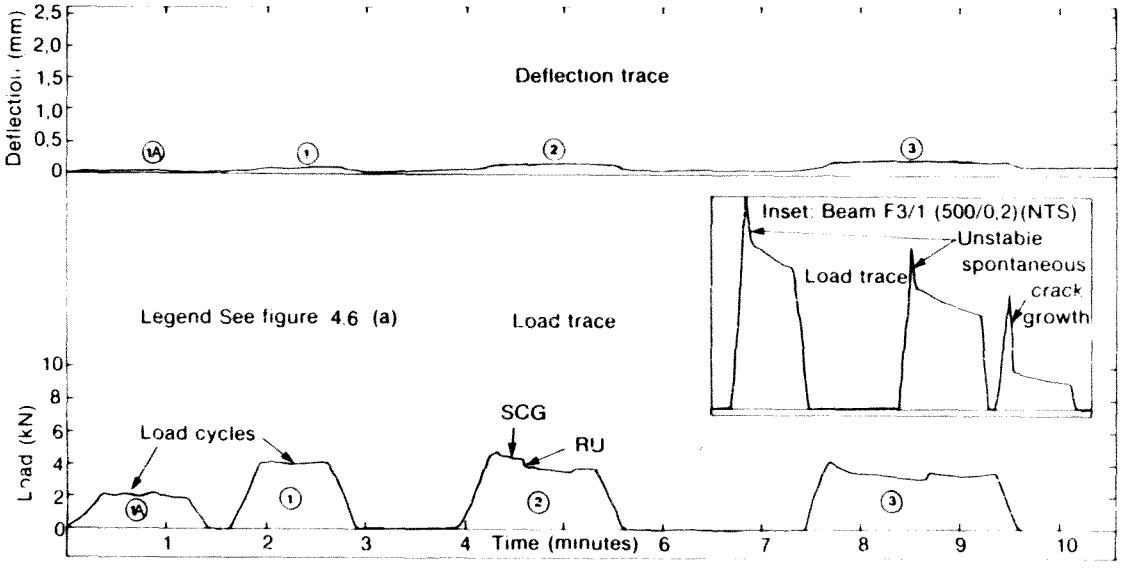

Figure 4.6(b) Portion of multi-channel test record for beam F3/15(200/0,4)



Figure 4.7 Progress of main crack with successive load cycles (F3/2(500/0,2))

Two final points bear mention here. The first concerns the question of drying of the beams during test, particularly for series F3 when the tests could run for up to thirty minutes or more. This effect was not investigated in the present work, but it was considered that since concrete as opposed to pure hardened cement paste was being tested, and that since the drying effect in thirty minutes could not have deeply penetrated the beam surfaces, the effect was probably not large. For the non load-cycled beams where failure occurred within two to three minutes, the effect was in all likelihood negligible. The second point was that it was realised that a more precise observation of the tip of a visible crack could have been achieved with the use of a small microscope, but unfortunately the test arrangement prevented this since there was insufficient space between the test machine columns and the specimen to insert a microscope. To compensate at least to some degree for this deficiency, spotlights were placed roughly one and a half metres from the beam and focussed on the painted surfaces, and great care was taken to observe the crack tip from as close as possible. The problem is really one of scale, since the observable depth of a crack will depend on the magnification being used and the surface condition of the specimen. For very fine work, high magnifications and polished surfaces are really required. In the context of the present work, however, fracture was being investigated in relatively large "macro-specimens" as opposed to small "micro-specimens" in which an error in crack depth determination would obviously be more serious. In addition, the use of strain readings at various distances above the lower face of a beam allowed the determination of a crack profile at each stage of loading, and it was possible to use this profile to assess the position of the crack tip, as well as the crack opening displacements at various points. This, it was felt, helped in overcoming the problem of crack depth measurement.

4.6 CONCLUDING SUMMARY

This chapter has provided details of the carrying out of fracture tests and related materials control tests. A total of 69 notched concrete beams of width 100mm and depth ranging from 100mm to 800mm were tested. Three series of tests were performed. Most of the beams were prismatic with a constant span/depth ratio of four. A number of the larger beams had variable sections to reduce mass. Small vertical "steps" were cast on the sloping faces to accommodate ultrasonic probes (for series F3 tests). The ratio of span/depth at mid-span was also four for these beams. "Demec" strain targets at mid-span and covering the beam height were fixed to one side of all beams on a 100mm gauge length for the final test series. Cast-in central notches with notch depth ratios of 0,2, 0,25, 0,4 or 0,5 were used. Materials were ordinary portland cement, quartzite crusher sand (Fineness modulus = 3,1 to 3,25) and 20mm crushed quartzite stone. Mix ratios by mass were 1 : 0,53 : 2,07 : 2,80 (cement : water : sand : stone).

Beams were loaded at mid-span and load-cycling was used to create stable crack growth. A load-cell and LVDT transducers produced continuous output of load versus mid-span deflection on an XY plotter, and on an independent strip-chart recorder. For the final test series, strain and ultrasonic readings were taken normally at the peak of each load cycle when visible crack depth was also very carefully observed.

5 BASIC TEST RESULTS

This chapter reports on two sets of test results: the first comprises the results of tests for the materials parameters that were used either for control purposes or for use in the fracture calculations; the second comprises basic results from the fracture tests such as load-deflection data, summary tables of maximum loads, certain relevant deflections, and areas under load-deflection curves. A discussion of notch-sensitivity, effects of beam support friction, and shapes of load-deflection curves is also included.

5.1 MATERIALS CONTROL TESTS

These tests were conducted to obtain material parameters, and as controls on material quality. A minimum of three 101,6mm cubes were cast simultaneously with each individual batch of fracture beams, and crushed at the same age as the companion beams, this age being between 28 to 30 days after casting. Modulus of rupture (MR) beams were cast for the batches of series F1 and F3. Certain MR beams for series F3 were notched in order to assess notch-sensitivity of the material. A "modified MR" could be obtained from these notched beams. In series F1 the MR beams were also used for measuring a flexural modulus of elasticity E. No MR beams were cast for series F2; elastic moduli for this series were obtained by cutting prisms (100x100x200mm) from the two ends of a failed 850mm long fracture beam, and testing these prisms in compression. Elastic moduli for series F3 were measured on 100x100x200mm prisms in compression; these prisms were cast together with the other control specimens for each batch used for fracture beams. However, in the end E

values for this series were inferred from the fracture beams themselves, for reasons discussed in 5.2.3.

5.1.1 CUBE COMPRESSION TESTS

These tests on 101,6mm cubes were carried out in accordance with SABS Standard Method 863[78]. The rate of loading was 15 MPa/min. The cubes, which were cured in the same way as the fracture beams, were first weighed before being tested in a saturated condition on either the Amsler or Tinius Olsen testing machines.

5.1.2 MODULUS OF RUPTURE TESTS (FLEXURAL STRENGTH)

SERIES F1

A single unnotched beam (101,6x101,6x610mm span) from each batch of fracture beams was used to obtain a flexural modulus of elasticity and a modulus of rupture. The tests were carried out in accordance with the general principles of SABS Standard Method 864[79], using third-point loading but with modifications as outlined in ref. 80 which is included in appendix C. The modifications involved using a beam with a span/depth ratio of six as opposed to the normal value of three, and instrumentation to measure the load-deflection relationship for the beam. The span/depth ratio of six was used to improve the sensitivity of the deflection readings. Two preliminary cycles of load were applied up to a maximum extreme fibre stress of about one-third of the estimated MR. A standard rate of loading and unloading of 1,5 MPa/min (extreme fibre stresses) was used. Corrections for the Seewald effect[81] and self-weight of the beam were applied to the results. The beams were tested in a saturated condition. The corrected formula for MR (third-point loading) used was:-

$$MR\ (MPa) = 1{,}0145\ \frac{F_{max}}{bd^2}\ S + 0{,}75.10^{-6}\ W_c\ \frac{S^2}{d} \qquad (5.1)$$

where W_c is the unit weight of the concrete (kN/m^3)
and S and d are beam support span and depth respectively (mm).

(In the above, the factor 1,0145 is the Seewald correction factor, and the second term is the self-weight term. Ref. 81, included in appendix C, contains details of the Seewald effect, which accounts for local stress distortions in the vicinity of a concentrated load).

SERIES F3

A different geometry for the MR tests was adopted, and 101,6x101,6x450mm beams were cast with each batch of fracture beams. These were tested in centre-point loading on a 400mm span. It was considered desirable to test MR beams of the same span/depth ratio as the small fracture beams so as to have a direct assessment of the notch-sensitivity of the material. Additional notched beams were also cast and tested together with the conventional MR beams. The initial notch depth ratios used were 0,2, 0,25 and 0,4. The net tensile stress at the root of the notch was calculated using the maximum load, including the self-weight. Notch-sensitivity was assessed in the same way for the larger fracture beams and the influence of specimen size was determined.

For the conventional MR beams, the Seewald effect (see appendix C) and self-weight were included in the formula as follows:-

$$MR\ (MPa) = 0{,}956\ \frac{3}{2}\ \frac{F_{max}}{bd^2}\ S + 0{,}75.10^{-6}\ W_c\ \frac{S^2}{d} \qquad (5.2)$$

(For notation, see under equation (5.1)).

For the notched MR beams the Seewald effect was ignored since it was negligible in comparison with the stress concentration effect of the notch. (Note also that the self-weight effect is small and is frequently neglected in this type of calculation).

5.1.3 MODULUS OF ELASTICITY TESTS

SERIES F1

These tests used the MR beams to also obtain flexural modulus of elasticity values from load-deflection measurements on a beam using third-point loading. The method of test is outlined in appendix C. Both shear and Seewald corrections were applied to the results. The formula used was:-

$$E = \frac{23}{1296} \frac{F}{\delta} \frac{S^3}{I} \left[1+\frac{216}{115}\left(\frac{d}{S}\right)^2\right] \times 1{,}052 \qquad (5.3)$$

where F/δ is the slope of the best-fit straight line drawn through the initial portion of the load-deflection curve (N/mm),
I is the second moment of area of the section (mm^4),
and the other symbols have their previously assigned meanings.

(The factor 1,052 is the Seewald correction factor, while the expression in square brackets accounts for the shear deflection. See appendix C).

SERIES F2 AND F3

Prism compression tests were used for elastic modulus values. Prisms for series F2 were cut from the two ends of a failed 850mm long fracture beam, and end faces were ground smooth on a facing wheel. The two prisms were kept saturated and the elastic modulus

tests were carried out immediately after grinding. Longitudinal strains were measured with a dial-gauge compressometer, and the method of test was generally in accordance with the principles of BS 1881:Part 5:1970[82]. The recommended rate of loading (15 MPa/min) was adhered to, and the accuracy of strain readings was $2,5.10^{-6}$. A photograph of a prism test is shown in figure 5.1. The tests were carried out on the Tinius-Olsen testing machine, with manual recording of load and strain.

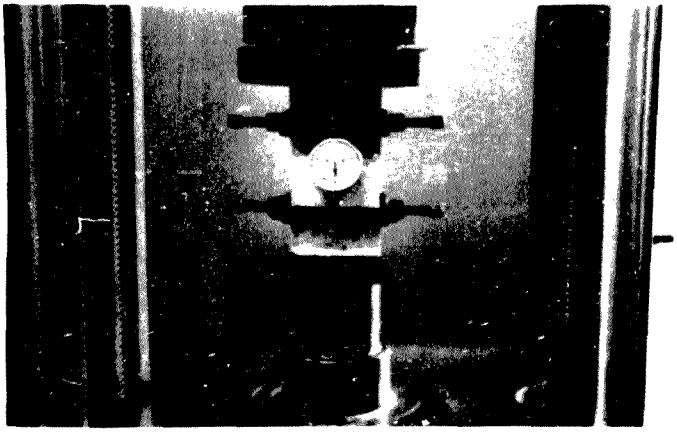

Figure 5.1 Prism compression test for elastic modulus (series F2)

For series F3, the prisms (100x100x200mm) were cast in steel moulds with each batch of fracture beams. A new strain rig was used which allowed longitudinal and transverse strains to be monitored continuously using LVDTs, the outputs of which were independently fed to the two Y channels of the XY recorder. The tests were conducted on the Tinius-Olsen machine, and the electronic load output was fed to the X-channel. A photograph of the strain rig attached to a specimen is shown in figure 5.2. Specimens were saturated at the time of test. The principles of BS 1881 : Part 5 : 1970[82] were adhered to for the test. The parameters were determined by using a secant value of the load-deformation slope between a lower stress of 1MPa and an upper stress of 10MPa.

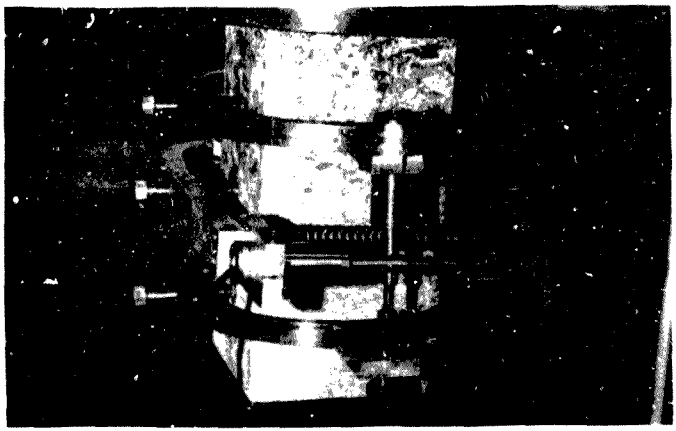

Figure 5.2 Prism compression test for elastic modulus and Poisson's ratio (series F3)

5.2 RESULTS FOR MATERIALS CONTROL TESTS

The results for the materials tests are given in table 5.1 such that the fracture beams associated with the particular materials tests can be identified. (The results for the notched MR beams for assessment of notch-sensitivity are given later in 5.4).

5.2.1 COMPRESSIVE STRENGTH

SERIES F1 AND F2

Series F1 and F2 concretes were cast in June/July and October of 1982 respectively. Specimens were cast and cured on the laboratory

Table 5.1 Results for materials control tests

(a) Series F1

Specimen identification	Age of test (d)	Mean concrete density (kg/m^3)	Cube strengths (MPa)		Modulus of rupture (MPa)	Modulus of elasticity (GPa)
F1/1(500/0,2) 2(500/0,2)	28	2450	39,23 41,37 39,43	$\bar{x}$ = 40,01	4,47	32,42
3(500/0,4) 4(500/0,4)	29	2435	40,98 40,98 40,30	$\bar{x}$ = 40,75	4,50	33,27
5(300/0,2) 6(300/0,2)	28	2406	32,65 31,97 33,13 33,03 32,26 32,65	$\bar{x}$ = 32,61 s=0,44	4,40	36,00
7(200/0,4) 8(200/0,4)	28	2405	27,42 30,32 26,93 28,77 28,68 30,03	$\bar{x}$ = 28,69 s=1,35	3,94	32,09
9(100/0,25) 10(100/0,25) 11(100/0,25)	28	2406	34,88 34,88 34,39 37,20	$\bar{x}$ = 35,34 s=1,26	5,27	-
12(100/0,4) 13(100/0,4) 14(100/0,4)	28	2445	71,35 68,88 69,31	$\bar{x}$ = 69,85	5,68	38,78

101,6x101,6x610mm span; third-point loading

101,6x101,6x610mm beams

Table 5.1 (Continued)

(b) Series F2

Specimen identification	Age of test (d)	Mean concrete density (kg/m³)	Cube strengths (MPa)		Modulus of rupture (MPa)		Modulus of elasticity (GPa)	
F2/1(800/0,2) 5(100/0,25) 6(100/0,25) 16(100/0,5) 17(100/0,5)	28	2451	37,10 42,92 45,05 37,88 39,82 39,62	$\bar{x}$ = 40,40 s=3,04	-		32,25 28,33	$\bar{x}$ = 30,29
2(800/0,4) 7(100/0,25) 8(100/0,25) 18(100/0,5) 19(100/0,5)	28	2500	35,17 35,65 36,04 34,39 37,88	$\bar{x}$ = 35,82 s=1,30	-	100 x 100 x 200mm prisms	32,87 31,28	$\bar{x}$ = 32,07
3(800/0,4) 9(100/0,4) 10(100/0,4) 20(100/0,5) 21(100/0,5)	28	2497	44,27 40,69 42,33 45,73 44,66	$\bar{x}$ = 43,54 s=2,01	-		-	
4(800/0,4) 11(100/0,4) 12(100/0,4) 22(100/0,5) 23(100/0,5)	28	2481	42,24 39,33 39,23 41,56 42,24	$\bar{x}$ = 40,92 s=1,52	-		30,63 32,32	$\bar{x}$ = 31,47
13(100/0,4) 14(100/0,4) 15(100/0,4) 24(100/0,5) 25(100/0,5) 26(100/0,5)	28	2422	40,78 41,08 40,59 42,24	$\bar{x}$ = 41,17 s=0,74	-		31,63 28,91 31,68	$\bar{x}$ = 30,74

Table 5.1 (Continued)

(c) Series F3

Specimen identification	Age at test (d)	Mean concrete density (kg/m³)	Cube strengths (MPa)	Modulus of rupture (MPa)	Modulus of elasticity (Poisson's ratio)
F3/1(500/0,2) 2(500/0,2)	28	2439	29,90 30,15 $\bar{x}$ = 32,16 30,53 30,77 29,86 s = 30,32 0,87	4,95 $\bar{x}$ = 4,73 4,80 4,73	25,24 (0,164) $\bar{x}$ = 20,56 22,75 (0,135) (0,157) 22,46 (0,173)
3(500/0,4) 4(500/0,4)	28/ 29	2445	32,12 31,15 $\bar{x}$ = 33,01 31,15 30,36 s = 29,93 30,32 1,20	5,54 $\bar{x}$ = 5,09 4,94 4,18	21,82 (0,150) $\bar{x}$ = 24,98 24,24 (0,147) (0,151) 25,93 (0,155)
5(300/0,2) 6(300/0,2) 7(300/0,25)	28/ 30	2443	31,10 $\bar{x}$ = 31,10 30,59 29,38 s = 30,79 0,82	4,64 $\bar{x}$ = 4,53 4,56 4,52	22,27 (0,157) $\bar{x}$ = 16,36 21,67 (0,201) (0,172) 26,38 (0,159)
8(300/0,25) 9(300/0,25) 10(300/0,4)	28	2428	29,91 $\bar{x}$ = 30,13 29,85 29,42 s = 29,94 0,30	4,73 $\bar{x}$ = 4,67 4,80 4,99	23,88 (0,160) $\bar{x}$ = 25,24 22,63 (0,125) (0,141) 18,77 (0,137)
11(300/0,4) 12(300/0,4) 27,28,29 (100/0,4)	28	2440	30,17 $\bar{x}$ = 31,84 31,20 32,01 s = 30,77 0,88	4,44	23,58 (0,166) $\bar{x}$ = 22,32 22,74 (0,170) (0,160) 22,32 (0,145)
13(200/0,2) 14(200/0,2) 15(200/0,4) 16(200/0,4) 21,22,23 (100/0,2)	29	2439	31,06 $\bar{x}$ = 31,10 30,84 29,64 s = 31,55 0,83	4,99	28,94 (0,164) $\bar{x}$ = 23,80 23,86 (0,119) (0,140) 18,85 (0,136)

101,6x101,6x400mm span; centre-point loading — 100 x 100 x 200mm prisms

Table 5.1 (Continued)

(c) Series F3 (Continued)

Specimen identification	Age at test (d)	Mean concrete density (kg/m³)	Cube strengths (MPa)		Modulus of ruptur (MPa)		Modulus of elasticity (Poisson's ratio)	
F3/17,18,19,20 (100/0,2)	28/29	24	31,72 31,46 31,37 29,98	$\bar{x}$ = 31,13 s = 0,78	4,45 4,88 4,25	$\bar{x}$ = 4,53	22,60 (0,241) 22,89 (0,146) 21,28 (0,153)	$\bar{x}$ = 22,26 (0,180)
24(100/0,25) 25(100/0,4) 26(100/0,4)	29/30	2435	32,30 32,36 33,13 30,09	$\bar{x}$ = 31,97 s = 1,31	5,08 5,36 3,99	$\bar{x}$ = 4,81	28,08 (0,184) 30,26 (0,228) 27,43 (0,188)	$\bar{x}$ = 28,59 (0,200)

101,6 x 101,6 x 406mm centre-point loading; 100 x 100 x 200mm prisms

Note $\bar{x}$ refers to the mean of a set of results

s refers to the sample standard deviation (only given where four or more results were available

floor since the fracture beams were generally too large to place in a curing tank, and since it was impossible to move the large specimens until they had gained strength. They were therefore subject to fluctuating temperatures in the laboratory. Mean laboratory temperatures during June/July (series F1) and during October (series F2) ere about 15°C and 20°C respectively. The results at the lower end of the strength spectrum for series F1 represent those cubes cast during June when the coldest temperatures prevailed. This factor is considered to have caused the variability of strength results. (Note that the unusually high results for specimens F1/12 to 14 are explained in appendix C. Suffice to say that two batches of concrete were cast, the first batch being used for cubes and MR/E beams and producing high strengths, and the second batch being used for the fracture beams which achieved correct design strength in line with other beams of this series)

SERIES F3

This series was cast approximately two and a half years after the earlier series, using different batches of cement and aggregates. The specimens were cast and cured on the floor of a curing room where the mean temperature was about 20°C, and there was very little temperature fluctuation. Consequently, the strength values were very consistent.

DISCUSSION

Table 5.2 shows the mean values and coefficients of variation (C.V.) for the cube tests, with the exception of the very high results for series F1 discussed in appendix C.

Author Alexander Mark Gavin
Name of thesis Fracture Of Plain Concrete: A Comparative Study Of Notched Beams Of Varying Depth. 1985

PUBLISHER:
University of the Witwatersrand, Johannesburg
©2013

LEGAL NOTICES:

Copyright Notice: All materials on the University of the Witwatersrand, Johannesburg Library website are protected by South African copyright law and may not be distributed, transmitted, displayed, or otherwise published in any format, without the prior written permission of the copyright owner.

Disclaimer and Terms of Use: Provided that you maintain all copyright and other notices contained therein, you may download material (one machine readable copy and one print copy per page) for your personal and/or educational non-commercial use only.

The University of the Witwatersrand, Johannesburg, is not responsible for any errors or omissions and excludes any and all liability for any errors in or omissions from the information on the Library website.